

### Key Points:

- The winter of 2018/19 saw unprecedentedly low sea ice cover in the Bering Strait region and Kotzebue Sound
- In-situ observations identify the ocean as the primary source of heat input to landfast ice in Kotzebue Sound throughout the winter
- River outflow is observed to promote ice formation and growth in the fall/winter, but contributes to ice melt and breakup in the spring

### Correspondence to:

C. R. Witte,  
cwitte@ldeo.columbia.edu

### Citation:

Witte, C. R., Zappa, C. J., Mahoney, A. R., Goodwin, J., Harris, C., Schaeffer, R. J., et al. (2021). The winter heat budget of sea ice in Kotzebue Sound: Residual ocean heat and the seasonal roles of river outflow. *Journal of Geophysical Research: Oceans*, 126, e2020JC016784. <https://doi.org/10.1029/2020JC016784>

Received 9 SEP 2020  
Accepted 18 FEB 2021

## The Winter Heat Budget of Sea Ice in Kotzebue Sound: Residual Ocean Heat and the Seasonal Roles of River Outflow

**Carson R. Witte<sup>1</sup> , Christopher J. Zappa<sup>1</sup> , Andrew R. Mahoney<sup>2</sup> , John Goodwin<sup>3</sup>, Cyrus Harris<sup>3</sup>, Robert J. Schaeffer<sup>3</sup>, Roswell Schaeffer Sr<sup>3</sup>, Sarah Betcher<sup>4</sup>, Donna D. W. Hauser<sup>5</sup> , Nathan J. M. Laxague<sup>1</sup> , Jessica M. Lindsay<sup>6</sup> , Ajit Subramaniam<sup>1</sup> , Kate E. Turner<sup>7</sup> , and Alex Whiting<sup>8</sup>**

<sup>1</sup>Lamont-Doherty Earth Observatory, Columbia University, Palisades, NY, USA, <sup>2</sup>University of Alaska Fairbanks, Geophysical Institute, Fairbanks, AK, USA, <sup>3</sup>Community of Kotzebue, Kotzebue, AK, USA, <sup>4</sup>Farthest North Films, Homer, AK, USA, <sup>5</sup>International Arctic Research Center, Fairbanks, AK, USA, <sup>6</sup>University of Washington Seattle Campus, Seattle, WA, USA, <sup>7</sup>National Institute of Water and Atmospheric Research, Wellington, New Zealand, <sup>8</sup>Native Village of Kotzebue, Kotzebue, AK, USA

**Abstract** The winters of 2017/18 and 2018/19 saw unprecedented sea ice minima in the Bering and Chukchi Seas. Kotzebue Sound, located in the southeastern corner of the Chukchi Sea, remained largely ice-free throughout the winter in a stark departure from both recorded history and Indigenous oral history. The only sea ice that persisted throughout the winter was landfast ice and most of this occupied a small corner of the Sound near the outflow of the Noatak and Kobuk Rivers. We present oceanographic and atmospheric time series from a heavily instrumented “ice-tethered observatory” located on this landfast ice above the river outflow channel. This observing station was deployed as part of the *Ikaagvik Sikukun* (Iñupiaq for “Ice Bridges”) project, in which hypotheses and subsequent observational programs were co-produced in partnership with an Indigenous Elder Advisory Council in Kotzebue. The measurements allow us to quantify the heat budget of the ice above the outflow channel, and identify the ocean as the primary source of heat contributing to thinning of the ice, which began in early February and accelerated rapidly before the recovery of the station in April of 2019. In concert with the ice-tethered observations, we use 2 years of oceanographic measurements from the mouth of Kotzebue Sound to characterize the influence of river outflow on the heat budget of the landfast ice, revealing a seasonal pattern in which the rivers promote ice formation and growth in the fall/winter, but help to drive melting of the ice in spring and early summer.

**Plain Language Summary** A study of sea ice was undertaken as part of the *Ikaagvik Sikukun* (Iñupiaq for “Ice Bridges”) project, in which scientific objectives were developed in partnership with an Indigenous Elder Advisory Council in Kotzebue, Alaska. One of these objectives was to explain why there was so little sea ice in Kotzebue Sound during the winters of 2017/18 and 2018/19. We set out to answer this question by making direct observations of the flow of heat into and out of the ice, and identified the ocean as the main source of heat driving ice melt during the winter. We also found that the outflow from several rivers was promoting ice growth during the fall and winter, but helping to drive ice melt in the spring and early summer.

## 1. Introduction

Arctic sea ice impacts the lives of people around the globe, from those who consider it home to those who have never seen it. It is a habitat for the hunted, a garden for the hungry, a bridge between places, a buffer against raging seas (Fang et al., 2018; Gearheard et al., 2013). It is a reflective cap on the top of the world that helps keep oceans cooling and jet streams moving (Francis & Vavrus, 2015; Screen & Simmonds, 2010). And as sea ice cover shrinks, it becomes ever more important to understand the intricacies of interactions between the atmosphere, the ice, and the water below. In this study, we present measurements of the processes affecting the formation and melt of coastal sea ice under the influence of a river outflow, made collaboratively by scientists and Indigenous Elders from the community of Kotzebue, Alaska. In doing so, we weave together potential implications of a rapidly warming Arctic at multiple scales, from livelihoods

in the local community to the future of coastal sea ice and its impact on Indigenous ways of life throughout the far north.

### 1.1. Basin-Scale Trends in Arctic Sea Ice and River Outflow

As greenhouse gas concentrations rise, the Arctic continues to warm at two times the global average due to a combination of increased poleward atmospheric heat transport and an ice-ocean albedo feedback loop in a phenomenon known as “Arctic Amplification” (Dai et al., 2019; Holland & Bitz, 2003), leading to losses in sea ice cover that already exceed early International Panel on Climate Change (IPCC) model predictions (Schweiger et al., 2011; Stroeve et al., 2007). Arctic sea ice has also been thinning significantly, with an 80% reduction in sea ice volume since 1980 (Laxon et al., 2013), and the virtual disappearance of thick multi-year ice that has survived more than three summers (Perovich et al., 2018). Current models predict a complete loss of summer sea ice cover in the Arctic by 2100 at the latest and potentially as soon as 2030 (Boé et al., 2009; Overland & Wang, 2013), a situation that would be unprecedented in the last million years based on the paleoclimate record (Overpeck et al., 2005).

With decreasing sea ice cover comes increasing sea surface temperature (SST), as more of the Arctic Ocean is exposed to solar insolation for longer periods throughout the year (Pistone et al., 2019). Coastal areas have seen the most warming, with SST anomalies of up to +4°C during recent summers in marginal seas such as the Chukchi, Beaufort, and Laptev (Timmermans & Ladd, 2019). This is in part due to riverine heat flux to the Arctic shelves, which has been increasing at a rate of 2.5 EJ/decade (Park et al., 2020), causing a ~10% reduction in basin-wide September sea ice extent from 1979 to 2012 (Whitefield et al., 2015). Over 10% of freshwater input to the world’s oceans occurs via river outflow into the Arctic (Aagaard & Carmack, 1989), carrying with it an average heat input of 3 TW, equivalent to 7% of the total oceanic heat inputs from the Atlantic and Pacific oceans (and 44% of the heat flux associated specifically with the Bering Strait through-flow; Park et al., 2020; Whitefield et al., 2015). A majority of the riverine heat flux occurs during spring and early summer, when river freshets driven by terrestrial warming deliver as much as 12 TW of heat to the largely ice-covered coastal shelves (Park et al., 2020; Whitefield et al., 2015). While the importance of Arctic rivers is only recently becoming understood, it is clear that they have the potential to significantly impact the heat budget of coastal sea ice on which many Arctic communities depend.

### 1.2. The Importance of Sea Ice to Arctic Communities

Far from being a desolate expanse of flat white, sea ice is considered by many who live on and around it to be a “beautiful garden” capable of supplying all the bounty a human civilization needs to survive (Gearheard et al., 2013). It holds a deeply spiritual place in Indigenous cultures throughout the Arctic, as a home, a hunting ground for pagophilic marine mammals and other critical traditional resources, and a bridge between isolated places and peoples (Gearheard et al., 2013). Loss of sea ice has dramatic implications for coastal Arctic communities, threatening food security, protection from erosion, physical and mental health, and ultimately Indigenous ways of life (Bronen, 2010). The deep ties between Arctic Indigenous cultures and sea ice mean that many Elders have tracked sea ice variables throughout their lives, making observations embedded in a worldview that speaks to long-term changes in the context of human-ice interaction (Eicken, 2010). Local Indigenous Knowledge is thus highly relevant to the identification of important research questions, design of effective sampling campaigns, assessment of a study within the context of interannual variability, and dissemination of information beyond a strictly scientific audience (Eicken, 2010). Partnership between scientists and Local Indigenous Knowledge holders in the design and execution of climate-related research has seen enormous growth in recent years (Klenk et al., 2017).

### 1.3. Bridging the Scientific and Indigenous Communities to Study Sea Ice Change

*Ikaagvik Sikukun* (Iñupiaq for “Ice Bridges”) is our project in Kotzebue, a town nestled within a large embayment on the northwest coast of Alaska (see Figures 1 and 3 for geographical context) that is home to the Qikiqtaġruŋmiut people. We have employed the knowledge co-production model of scientific research (e.g., Behe & Daniel, 2018), which is predicated on the involvement of the local community in the design and direction of a research project from its inception, emphasizing a focus on objectives relevant to both the

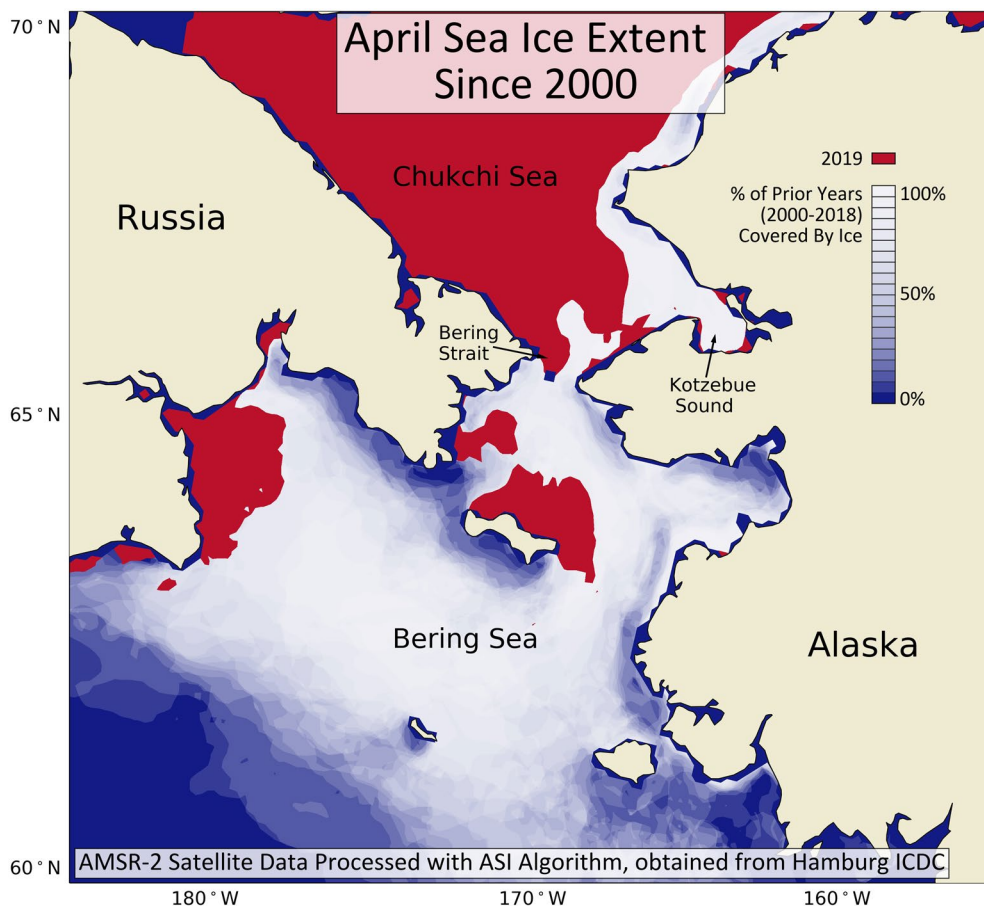


**Figure 1.** Sea ice cover (>70%) in the Chukchi and Bering Seas for every April since the year 2000. Each year is plotted as a transparent white layer, building up a qualitative climatological map over which 2019 April sea ice cover is shown in red. Data from Hamburg ICDC 12.5 km 5-day median-filtered ASI-SSMI product (<http://icdc.cen.uni-hamburg.de>).

community in which the research is taking place as well as the broader scientific community. The first year of the project was therefore dedicated to co-developing a series of five overarching research questions under the guidance of an Indigenous Elder Advisory Council comprised of co-authors John Goodwin, Cyrus Harris, Ross Schaeffer, and Robert Schaeffer. These questions reflect the holistic concerns of local community members whose livelihoods and lifestyles are intimately linked with the sea ice of Kotzebue Sound. Each question is multifaceted and requires bringing together new data and knowledge from a variety of disciplines.

After our first winter of observations in 2018, during which Kotzebue Sound was largely ice-free in a stark departure from both long-term Indigenous oral history and the near-term historical satellite record, the advisory council put forward a sixth question:

*Why was there so little sea ice in Kotzebue Sound in 2018 (and 2019)?*

The knowledge co-production framework enabled us to respond to this new development within the parameters of our existing project, resulting in the measurements and analysis presented here. As we attempt to provide an in-depth answer to the above question, we will also touch on implications for answering two of the other research questions developed by the *Ikaġvik Sikukun* team:

*What determines ice transport processes in Kotzebue Sound? What environmental factors control the length of the ugruk (Iñupiaq for bearded seal) hunting season in Kotzebue Sound?*

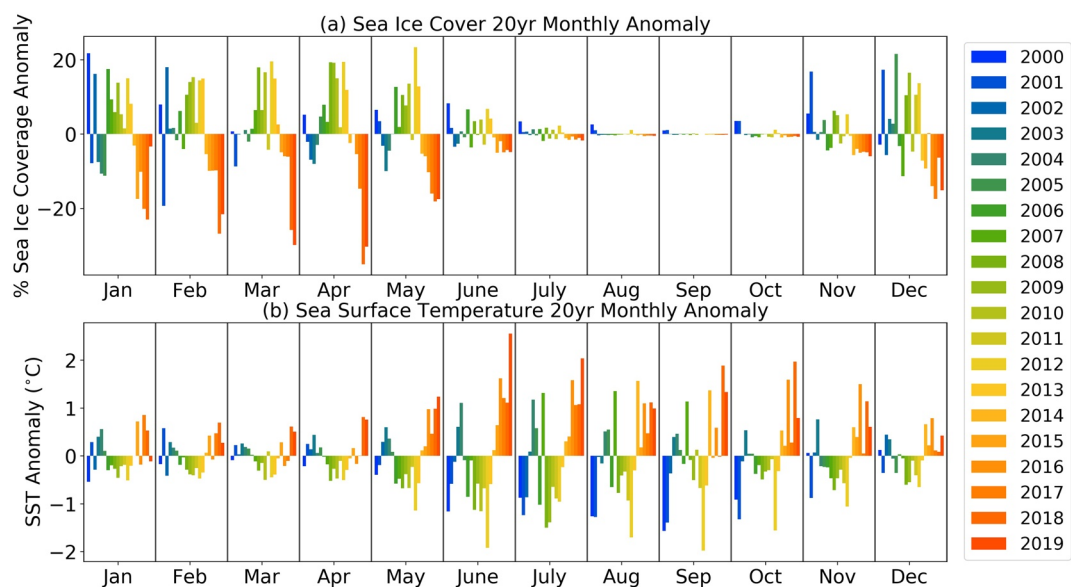


**Figure 2.** Monthly anomalies in (a) sea ice cover and (b) sea surface temperature in the Chukchi and Bering seas, relative to the 2000–2019 mean. Sea ice data from Hamburg ICDC 12.5 km 5-day median-filtered ASI-SSMI product ([icdc.cen.uni-hamburg.de](http://icdc.cen.uni-hamburg.de)). SST data from NOAA  $\frac{1}{4}^{\circ}$  Daily OISST Reynolds interpolated product ([ncdc.noaa.gov/oisst](http://ncdc.noaa.gov/oisst)). Both data sets were averaged over the geographical region depicted in Figure 1.

These questions are reflective of the fundamental (and cross-disciplinary) ties between sea ice and Indigenous ways of life in Kotzebue Sound, where the circulation patterns of ice affect access to hunting grounds for critical subsistence resources like *ugruk*, whose lives are themselves deeply intertwined with the ice.

#### 1.4. Coastal Oceanography of Kotzebue Sound

Kotzebue Sound is a large, shallow embayment located just north of the Bering Strait along the Alaska coast, with an areal extent of  $\sim 5,000 \text{ km}^2$  and water depths ranging mostly between 10 and 20 m. Circulation in the Sound is influenced by the Alaska Coastal Current (ACC), which brings warm water north through the Bering Strait and along the Alaska coast into the Beaufort Sea. While most of the ACC flows past the mouth of Kotzebue Sound, some of the surface waters are deflected into the Sound, eventually leaving the Sound at its northern edge and rejoining the main branch of the ACC (LaFond, 1954). The relatively warm waters of Kotzebue Sound are thought to be a major heat source to the ACC north of the Bering Strait (Ahlness & Garrison, 1984). There are locally significant freshwater inputs to Kotzebue Sound from the Noatak and Kobuk rivers, and low salinity water is observed to depart the Sound at its northern edge, where salinity gradually increases with westward distance from the river mouths (Coachman et al., 1975). Although relatively little is known about the seasonal cycle of outflow from these rivers, median statistics for 37 years of intermittent observations on the Kobuk river reveal two yearly discharge peaks, one in mid-May and the second in mid-August (USGS National Water Information System: <https://nwis.waterdata.usgs.gov>, Station ID 15744500).

#### 1.5. Unprecedented Sea Ice Minima in the Bering Strait Region During 2018 and 2019

The winter of 2019 proved similar to 2018, with sea ice largely absent from the Bering Sea and Kotzebue Sound by April (Figure 1). To complement the qualitative spatial climatology shown in Figure 1, Figure 2 provides a temporal perspective on monthly anomalies in both sea ice cover and SST over the 20 preceding years, quantifying the unusually warm and ice-free conditions in the Bering Strait region that formed the backdrop for this study. Our Elder Advisors have shared with us that up until about 20 years ago, Kotzebue Sound was entirely filled with “landlocked” landfast ice that was 5 or 6 ft. thick throughout the winter, and it was possible to travel safely over the ice between any two points on the shores of Kotzebue Sound. Since

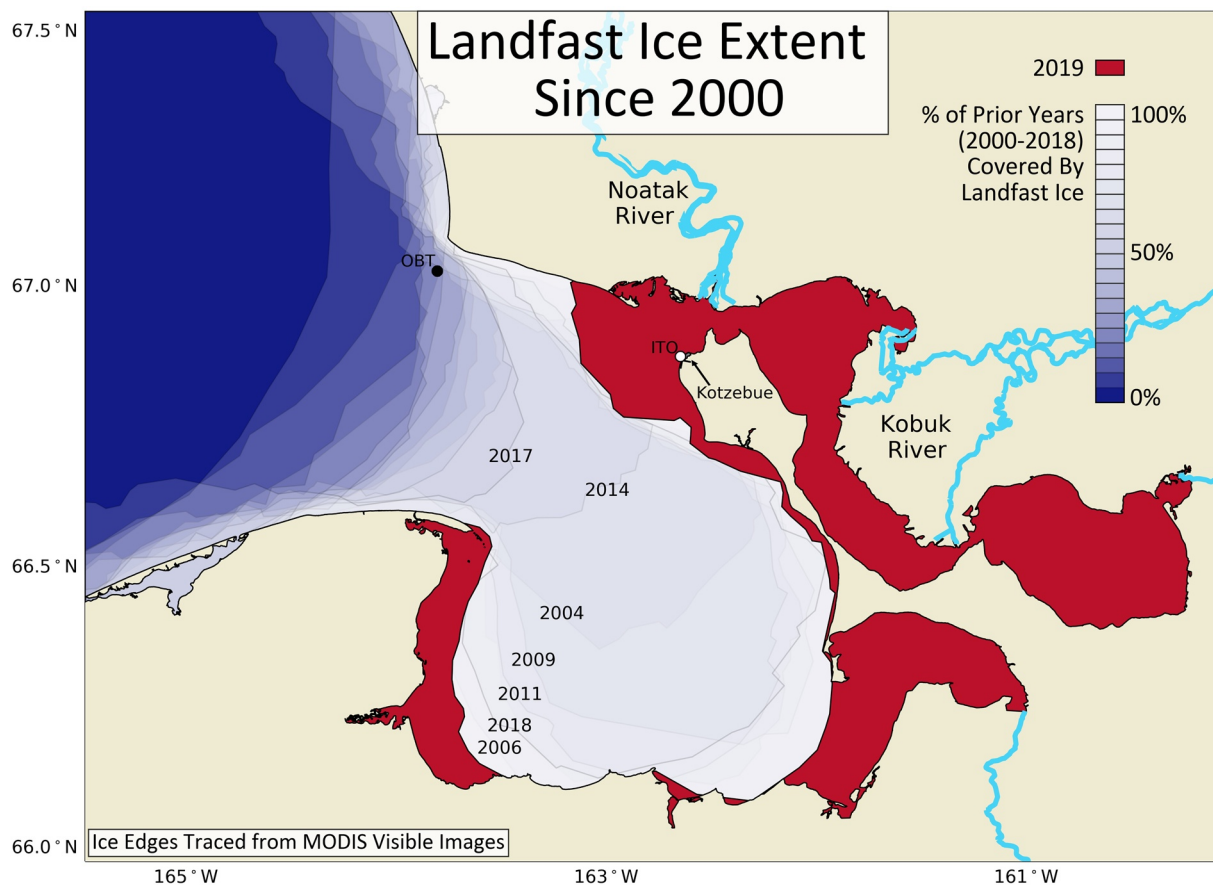


**Figure 3.** Qualitative climatological map of landfast ice in Kotzebue Sound since 2000, plotted following the same color scheme as Figure 1. The landfast ice edge for each year was defined as an ice edge that was contiguous with the shoreline and remained stationary between its formation in February/March and the breakup of the entire sound in May/June. These edges were visually identified and hand-traced from MODIS visible images in a GIS program. Other years when the landfast ice edge was well inside the sound are labeled. For context, the locations of the ice-tethered observatory (ITO, white circle) and ocean bottom tripod (OBT, black circle) are also shown.

the turn of the century, our Elder Advisors have experienced increasingly marginal ice conditions and shortening cold spells, and rarely encounter winter air temperatures of  $-50^{\circ}\text{F}$ , which used to be commonplace when they were growing up.

From 1996 to 2008, Kotzebue Sound was filled with “landlocked” landfast ice from the beginning of February until the end of May ( $\pm 1$  week, on average) as reported by Mahoney et al. (2014) based on satellite analysis. Following a scheme similar to Figure 1, Figure 3 provides a qualitative climatological perspective on landfast ice in Kotzebue Sound throughout the 21st century. Some recent years have seen reduced landfast ice extent in Kotzebue Sound, with the seaward portion of the Sound occupied by mobile pack ice from the Chukchi Sea. In 2019, there was very little pack ice in the southeast Chukchi Sea, and much of the Sound remained open water through the winter, resulting in the lowest ice year in the living memory of our Elder Advisors. Landfast ice persisted only in the margins, with the largest piece occupying the northeast corner of the Sound adjacent to the town of Kotzebue. This region is characterized by extremely shallow bathymetry, with the exception of a 12-m deep channel in which the outflows from the Noatak and Kobuk rivers converge and enter the Sound. We learned from our Elder Advisors that breakup of landfast ice throughout Kotzebue Sound has historically been preceded by the melting of ice directly above the river outflow channel (see Figure 4 for satellite imagery of breakup from three different years, including 2019). The persistence of landfast ice in the very same region that historically tends to break up first suggested the interplay between ocean and river water as a crucial factor in the thermodynamics of Kotzebue Sound sea ice. We therefore sought to quantify the relative roles of atmosphere, ocean, and river in the heat budget of the landfast ice over the course of an anomalous winter season.

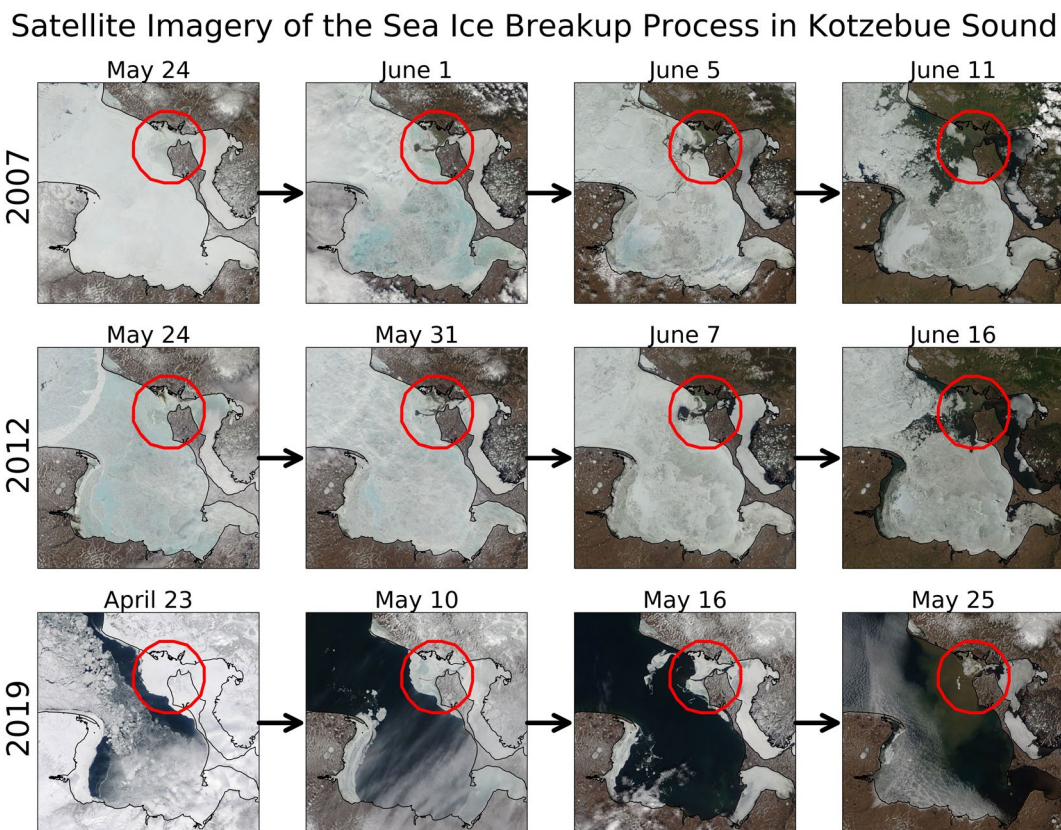


**Figure 4.** MODIS Visible satellite images showing the ice breakup process in Kotzebue Sound for 3 recent years. 2007 and 2012 were chosen for their lack of cloud cover, while 2019 was the year of this study, during which the ice breakup process occurred much earlier than previous years. Note the appearance of the river channel in the northeast corner of the Sound (circled in red) as a precursor to further breakup.

## 2. Methods

### 2.1. Ice-Tethered Observatory and Ocean Bottom Tripod

We deployed two measurement stations for this project, pictured in Figure 5. The first was a suite of ocean, ice, and atmospheric measurement instruments installed ~560 m from shore on the ice above the 12 m deep outflow channel of the Kobuk and Noatak rivers from January 7, 2019 to April 1, 2019. This “Ice-Tethered Observatory” (ITO) measured air temperature, humidity, and pressure; wind speed & direction; net shortwave (SW) and longwave (LW) radiation; snow and ice thickness; and under-ice water temperature, salinity, and current profiles. The ITO was designed to measure the heat budget of the snow/ice layer from both above and below. Table 1 details the automated instrumentation used on both stations, including accuracy specifications as well as deployment height/depth. The ITO also included snow stakes and hotwire gauges (Mahoney et al., 2009, 2021) where snow depth and ice thickness were measured on an approximately weekly basis by residents of Kotzebue, including co-authors Robert J. Schaeffer and Alex Whiting. As a complement to the ITO, downwelling shortwave and longwave radiation were also measured by a heated pyranometer & heated pyrgeometer installed on a tower above the Fish & Wildlife Service building in Kotzebue, ~720 m ESE of the ITO.

The second station was an “Ocean Bottom Tripod” (OBT), which took measurements of temperature, salinity, and ocean currents at the mouth of Kotzebue Sound. The OBT was deployed from September 15, 2017 to June 18, 2019, with a gap between August 24 and September 10, 2018, to put new batteries in the instruments. The goal of deploying the OBT was to gain insight into the interactions between the river outflow, Kotzebue Sound, and the greater Chukchi Sea; it was therefore placed in the northern section of the Sound mouth, this being identified by our Elder Advisors as the location of the primary outflow from

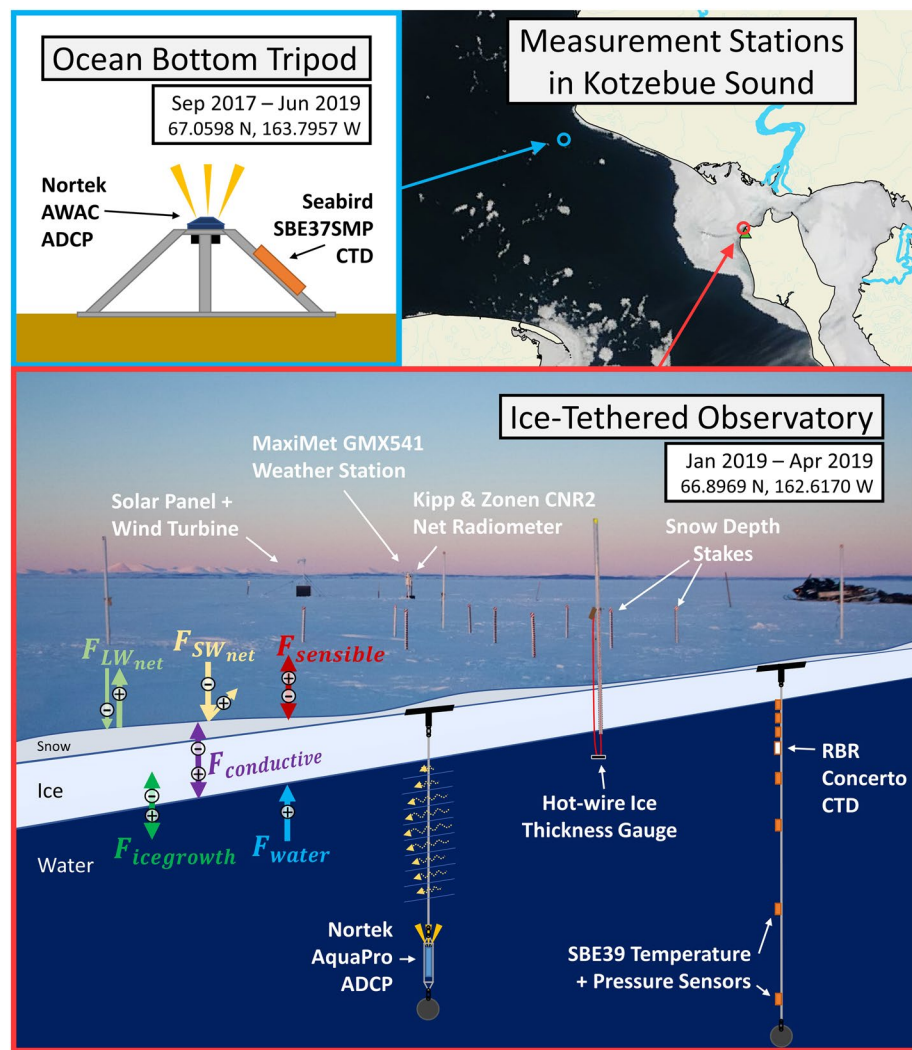


**Figure 5.** Locations, deployment durations, and schematics of the ocean bottom tripod (OBT, blue circle) and ice-tethered observatory (ITO, red circle) measurement stations in Kotzebue Sound. The OBT featured measurements of water temperature, salinity, and current profiles. The ITO featured measurements of net radiative fluxes, air temperature, humidity, pressure, wind speed, and solar insolation above the ice. Below the ice, moorings measured water temperature, salinity, and current profiles. Repeated measurements of snow and ice thickness were made by local observers on a weekly basis using calibrated stakes. Also shown are sign conventions for the flux balances at the water-ice and snow-air interface, for reference with Figure 9. The satellite image in the top right is from MODIS Visible, May 7, 2019. The green triangle adjacent to the red circle on the map indicates the location of the hemispheric radiometers installed above the Fish & Wildlife Service (FWS) building.

the Sound. Furthermore, visible satellite imagery from previous summers showed large sediment plumes flowing down the river channel and passing out of the Sound over our intended deployment site, bolstering our confidence that the OBT was being placed downstream of river outflow.

## 2.2. Estimating Fluxes at the Snow-Atmosphere Interface

Following Maykut (1986), we can write the surface heat balance for young ice with a layer of snow on top of it as:

$$F_{\text{netSW}} + F_{\text{netLW}} + F_{\text{sensible}} + F_{\text{latent}} + F_{\text{snowmelt}} + F_{\text{conductive}} = 0 \quad (1)$$

where fluxes ( $F$ ) are defined as positive away from the snow surface, and negative into the snow surface.  $F_{\text{netSW}}$  and  $F_{\text{netLW}}$  are the net radiative fluxes of shortwave (solar) and longwave (infrared) energy at the

**Table 1**

*Summary of All Sensors Used in This Experiment, Including Deployment Location, Height/Depth, Physical Parameters Being Measured, and Manufacturer-Specified Accuracy*

Sensor	Location	Height above ice surface (m)	Parameters measured	Measurement accuracy
Gill MaxiMet GMX541 Weather Station	Ice-tethered observatory	1	SW radiation ( $\text{W}/\text{m}^2$ ) 2-D wind speed (m/s) 2-D wind direction (deg.) Air temperature ( $^\circ\text{C}$ ) Air humidity (g/kg) Air pressure (hPa)	ISO 9060 2nd Class $\pm 3\%$ $\pm 3^\circ$ $\pm 0.3^\circ\text{C}$ @ $20^\circ\text{C}$ $\pm 2\%$ @ $20^\circ\text{C}$ $\pm 0.5 \text{ hPa}$ @ $25^\circ\text{C}$
Kipp & Zonen CNR2 Net Radiometer	Ice-tethered observatory	1	Net SW radiation ( $\text{W}/\text{m}^2$ ) Net LW radiation ( $\text{W}/\text{m}^2$ )	$\pm 10\%$ $\pm 10\%$
RBR Concerto CTD	Ice-tethered observatory	-3	Conductivity (mS/cm) Water temperature ( $^\circ\text{C}$ ) Pressure (dbar)	$\pm 0.013 \text{ mS/cm}$ $\pm 0.002^\circ\text{C}$ $\pm 0.01 \text{ dbar}$
Seabird SBE39 TD (x7)	Ice-tethered observatory	-1.5, -2, -2.5, -4, -6, -8, -10	Water temperature ( $^\circ\text{C}$ ) Pressure (dbar)	$\pm 0.002^\circ\text{C}$ $\pm 1 \text{ dbar}$
Nortek Aquadopp Profiler 2 MHz ADCP	Ice-tethered observatory	-6	3-D current profile, 0.5 m vertical bins (m/s) Water temperature ( $^\circ\text{C}$ ) Pressure (dbar)	$\pm 1\%$ of measured value $\pm 0.5 \text{ cm/s}$ $\pm 0.1^\circ\text{C}$ $\pm 0.25 \text{ dbar}$
Seabird SBE37SMP CTD	Ocean bottom tripod	-17	Conductivity (mS/cm) Water temperature ( $^\circ\text{C}$ ) Pressure (dbar)	$\pm 0.006 \text{ mS/cm}$ $\pm 0.002^\circ\text{C}$ $\pm 2 \text{ dbar}$
Nortek AWAC 400 kHz ADCP	Ocean bottom tripod	-17	3-D current profile, 1 m vertical bins (m/s) Water temperature ( $^\circ\text{C}$ ) Pressure (dbar)	$\pm 1\%$ of measured value $\pm 0.5 \text{ cm/s}$ $\pm 0.1^\circ\text{C}$ $\pm 0.25 \text{ dbar}$
Kipp & Zonen CGR4 Pyrgeometer	FWS building	20	LW radiation ( $\text{W}/\text{m}^2$ )	<5 $\text{W}/\text{m}^2$
Kipp & Zonen CMP22 Pyranometer	FWS building	20	SW radiation ( $\text{W}/\text{m}^2$ )	<5 $\text{W}/\text{m}^2$

surface. The sensible heat flux can be robustly parameterized in terms of the wind speed  $u(z)$  and the difference between the air temperature  $T_a$  and the snow surface temperature  $T_0$ :

$$F_{\text{sensible}} = \rho_a c_p C_{H(z)} u(z) [T_0 - T_a] \quad (2)$$

where  $\rho_a$  is the density of the air,  $c_p$  is the specific heat capacity of air, and  $C_{H(z)}$  is the bulk atmospheric heat transfer coefficient for a snow surface on top of sea ice (given a measurement height  $z$  for air temperature and wind speed). We use a value of  $C_{H(1m)} = 2 \times 10^{-3}$  following (Andreas, 2002; Andreas et al., 2005; Kondo & Yamazawa, 1986).

The latent heat flux has been observed to be negligible (< 1  $\text{W}/\text{m}^2$ ) from November to March over sea ice in the Arctic (Maykut, 1986), so  $F_{\text{latent}}$  is assumed to be zero here. Also, the heat flux associated with snowmelt,  $F_{\text{snowmelt}} = [\rho_s L_s dh_s/dt]_0$  (where  $\rho_s$  is the snow density,  $L_s$  is the latent heat of fusion of snow, and  $h_s$  is the depth of snow), is equal to zero as long as the snow surface temperature  $T_0$  is below freezing, and during this experiment proved negligible (< 0.1  $\text{W}/\text{m}^2$ ) in rare cases when  $T_0$  was above freezing.

Finally, the conductive heat flux can be calculated from the temperature gradient across the ice and snow, which we assume to be linear in thin young ice with relatively little snow cover (Maykut, 1986). We also assume that the base of the ice is at the freezing point  $T_f$ , given that it is in contact with water directly beneath it. The thermal conductivities of ice and snow,  $k_i = 2.1\text{W/m}\cdot\text{K}$  and  $k_s = 0.3\text{W/m}\cdot\text{K}$ , respectively (from Maykut, 1986), must be scaled by the relative thicknesses of the ice and snow layers  $h_i$  and  $h_s$  to get one expression for the conductive flux across the combined snow and ice layer:

$$F_{\text{conductive}} = \frac{\left[ T_0 - T_f \right]}{\cancel{h_i} \cancel{k_i} + \cancel{h_s} \cancel{k_s}}, \quad (3)$$

Equation 1 can now be reduced to:

$$F_{\text{netSW}} + F_{\text{netLW}} + \rho_a c_p C_{H(z)} u(z) [T_0 - T_a] + \frac{\left[ T_0 - T_f \right]}{\cancel{h_i} \cancel{k_i} + \cancel{h_s} \cancel{k_s}} = 0. \quad (4)$$

All of the variables in Equation 4 except the snow surface temperature  $T_0$  can be directly measured by the CNR2 net radiometer, MaxiMet weather station, snow stakes, and hotwire gauges. Thus, we rearrange Equation 4 to solve for  $T_0$ . From there, we can calculate the sensible and conductive heat fluxes at the surface.

### 2.3. Estimating Fluxes at the Water-Ice Interface

We can express the heat balance at the water-ice interface, again following Maykut (1986), as:

$$F_{\text{icegrowth}} + F_{\text{water}} + F_{\text{conductive}} = 0 \quad (5)$$

where  $F_{\text{icegrowth}} = \rho_i L_i dh_i/dt$  ( $\rho_i$  is the ice density,  $L_i$  is the latent heat of fusion, and  $h_i$  is the thickness of ice) is the latent heat required to melt or grow sea ice. The oceanic heat flux into the bottom of the ice is calculated as:

$$F_{\text{water}} = \rho_w c_p \langle w' T' \rangle_0 \quad (6)$$

where  $\rho_w$  is the water density,  $c_p$  is the water's specific heat capacity, and  $\langle w' T' \rangle_0$  is the covariance of the turbulent fluctuations in vertical velocity and temperature at the ice-bottom boundary (the ' superscript denotes a signal with the mean removed, leaving only the turbulent fluctuations). In practice,  $\langle w' T' \rangle_0$  is difficult and costly to measure directly, so we rely on empirical parameterizations that relate the direct covariance formulation of Equation 6 to one composed of readily observable bulk properties. Similar to the parameterization of sensible heat flux at the snow-air interface, the water-ice heat flux can be parameterized following McPhee (1992) in terms of:

1. The temperature gradient ( $\Delta T$ ) across the boundary layer beneath the ice, that is, the elevation of the bulk ocean temperature above its freezing point:

$$\Delta T = T_{\text{bulk}} - T_{\text{freezing}}(S_{\text{bulk}}) \quad (7)$$

where the freezing point is calculated as a function of bulk salinity.

2. Turbulent mixing within the boundary layer, characterized by the friction velocity at the interface ( $u_{*0}$ ), which is calculated following the “law of the wall” (McPhee, 2008) assuming a logarithmic velocity profile beneath the ice-bottom boundary:

$$u_{*0} = \kappa \frac{u(z) - u(z_0)}{\ln(\cancel{z} \cancel{z_0})} \quad (8)$$

where  $u(z)$  is the velocity measured at depth  $z$  from the ice-bottom boundary,  $z_0$  is the roughness length,  $u(z_0)$  is assumed to be zero because the ice is stationary, and  $\kappa = 0.4$  is the Von Karman constant. We can apply a semilogarithmic fit to measurements of the velocity profile within the under-ice boundary layer to determine  $u_{*0}$  and the roughness length  $z_0$  (as in McGillis et al., 2004; Equation 10).

We must also introduce a non-dimensionalized heat transfer coefficient, or Stanton number ( $St_*$ ), which can be conceptualized as an intrinsic property of the water-ice boundary layer that dictates the relationship between friction velocity, under-ice temperature gradient, and the resulting heat flux into the ice:

$$St_* = \frac{\langle w'T' \rangle_0}{u_{*0} \Delta T}. \quad (9)$$

Combining Equations 6–9 results in a new expression for the water-ice heat flux:

$$F_{\text{water}} = \rho c_p \langle w'T' \rangle_0 = \rho c_p (St_* u_{*0} \Delta T). \quad (10)$$

Assuming that the Stanton number is constant, we have now expressed the water-ice heat flux in terms of properties measurable with the oceanographic instrumentation installed at the ice-tethered observatory (ADCP and CTDs).

The assumption that  $St_*$  is a constant ignores the potential importance of molecular viscosity and diffusivity near the water-ice interface. Ice melt—which can also raise the freezing point directly beneath the ice due to its low salinity—could suppress turbulent exchange by stabilizing the boundary layer and creating a non-negligible layer in which molecular processes dominate. Indeed, more complex formulas incorporating Stanton number dependence on roughness length and molecular properties such as viscosity have been proposed (McPhee, 1987; Owen & Thomson, 1963; Yaglom & Kader, 1974). However, direct covariance data from six separate experiments observing different ranges of thermodynamic forcing and under-ice surface roughness have yielded remarkably consistent values for  $St_*$  (McPhee et al., 1999). Furthermore, the Reynolds number dependent formulation put forth by Yaglom and Kader (1974) does not fit the data well, overestimating  $St_*$  for hydraulically smoother ice bottoms and underestimating it for rougher ones, leading McPhee et al. (1999) to conclude that “over the range of roughness Reynolds number likely to be encountered under sea ice, constant [ $St_*$ ] is a better choice.”

Finally, the conductive heat flux at the water-ice boundary is the same as the conductive heat flux at the snow-air boundary, as conductive flux is assumed to be constant across young ice with relatively thin snow cover (Maykut, 1986).  $F_{\text{conductive}}$  thus provides us with a means to relate the independent measurements being made of heat flux above and below the ice. Heat storage within the ice and snow is typically at least an order of magnitude smaller than the heat required to grow or melt the ice and we therefore neglect it here.

### 3. Results

#### 3.1. Ice-Tethered Observatory Data

Data collected from the ITO are summarized in Figure 6. Winds (a) were predominantly easterly throughout the study period, with several distinct westerly wind events indicated by warmer colors. Maximum wind speeds were generally higher in January and February than March, and low wind speeds were often associated with a drop in humidity (b) and air temperature (c). The air temperature approached 0°C during several periods in January and February, and was often above the climatological maximum air temperature of  $-14.6^{\circ}\text{C}$  for JFM at Kotzebue airport during the period 1949–2005 (data available at NOAA National Centers for Environmental Information (NCEI) Climate Data Online (CDO) Tool: <https://www.ncdc.noaa.gov/cdo-web/>, Station WBAN:26616). Periods with especially cold air temperatures (i.e., below  $-20^{\circ}\text{C}$ ) were associated with relatively low down-welling longwave radiation (d), indicating clear sky conditions and a large net loss of radiative energy from the snow surface (e). Downwelling SW measured at the ITO and FWS building are practically indistinguishable, enhancing our confidence in the measurements. However, the surface albedo (f), calculated from the daily mean difference between down-welling (d) and net (e) shortwave radiation, is still likely biased high during January and February due to the limitations of the instruments in generating a cosine response at very low sun angles. The decline in albedo at the end of March corresponds to a sustained period of air temperatures at or near 0°C, suggesting the onset of surface melt. Snow depth (g) increased dramatically between the measurements taken on February 5 and 13, due to a large storm arriving from the northwest on February 13, as reflected by reports from local observers and borne out in the wind time series. Increased snow depth is expected to exert an insulating effect on the ice, and indeed the arrival of the storm coincided with the end of ice bottom growth (g).

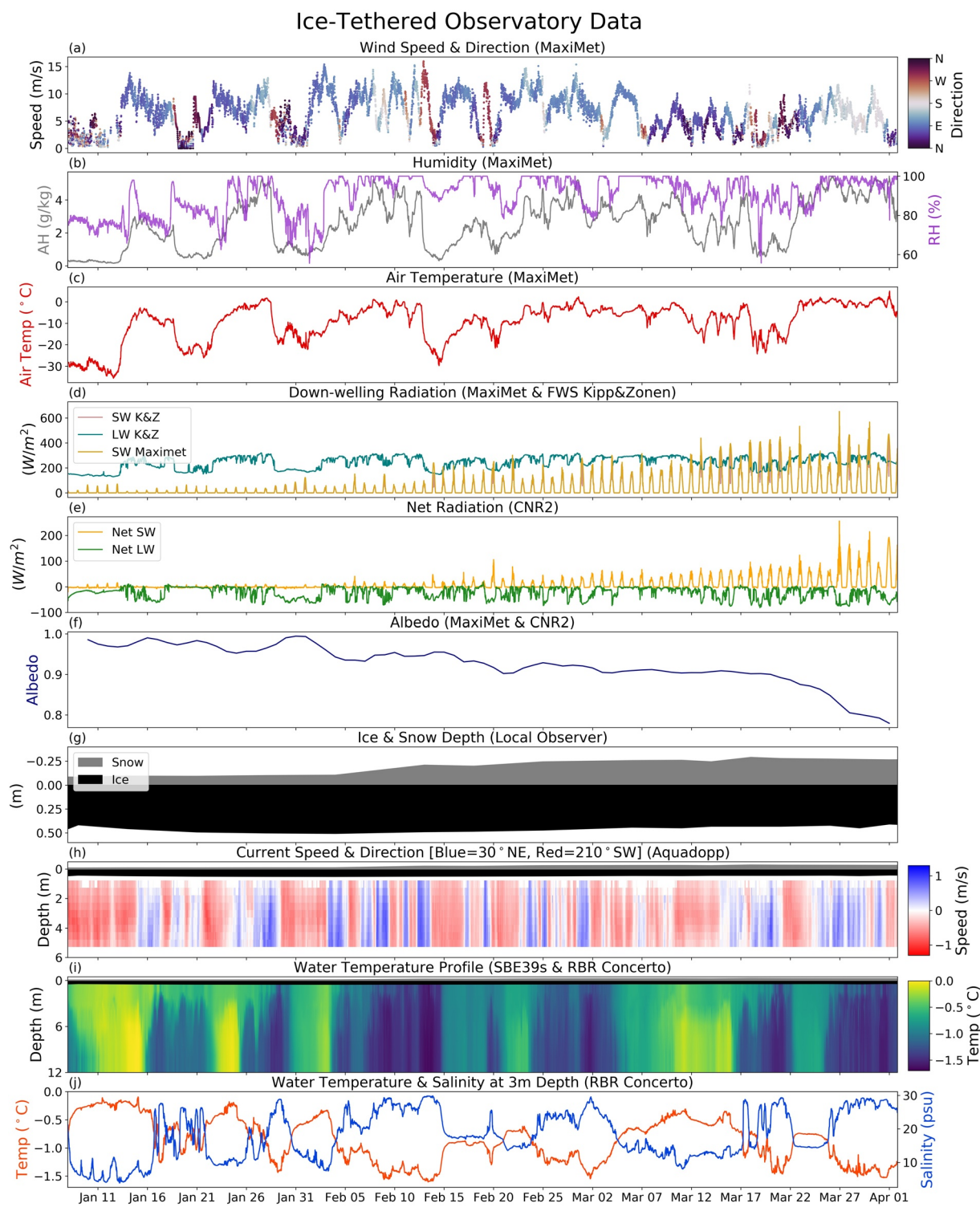


**Figure 6.** Summary of all measurements made on the ice-tethered observatory (ITO): (a) wind speed and direction, (b) absolute & relative humidity, (c) air temperature, (d) down-welling SW radiation, plus down-welling longwave (LW) and shortwave (SW) radiation measurements from a tower above the Fish and Wildlife Service (FWS) building in Kotzebue, (e) net LW and SW radiation, (f) albedo calculated by differencing the CNR2 net radiometer and down-welling SW sensor on the MaxiMet, (g) ice & snow depth, (h) current speed-oriented along its primary (NE–SW) axis, (i) full-depth water temperature profile, and (j) water temperature & salinity at 3 m depth.

Currents in the river outflow channel below the ice (h) were highly bi-modal along a 30–210° (northeast–southwest) axis, with flow originating either from the ocean (northeastward flow) or from the river mouths (southwestward flow). 90% of all current direction measurements were within ±40° of the central flow axis. The tidal signal is relatively weak—a power spectral density analysis of the depth-averaged current does show a small peak at a 12.8-h period, corresponding to the principal lunar semidiurnal (M2) harmonic constituent, which is the predominant harmonic constituent driving Kotzebue Sound tides. However, tidal influence is dwarfed by longer-period fluctuations, which are likely driven by a complex interplay between wind forcing and river outflow. Water temperature (i) varied between the freezing points of freshwater (0°C) and saltwater (−1.8°C), with southwest flow generally bringing warmer water. Water temperature and salinity (j) were highly anti-correlated (−0.97), as would be expected at the intersection between a fresh river and a salty ocean at their respective freezing points. However, there are also points throughout the time series (such as the first week) when salinity increases are observed without a coincident decrease in water temperature. It is moments like these that have the potential to deliver sensible heat to the ice bottom.

### 3.2. Water Properties Under the Ice

The relationships between flow direction and water properties are further explored in Figure 7. Unsurprisingly, the direction of flow corresponded closely to the sign of the temporal derivative of salinity (Figure 7b), with northeastward flow bringing saltier ocean water and southwestward flow bringing fresher river water. However, the flow did not necessarily need to reverse direction entirely for there to be a salinity change. The blue-shaded and green-shaded regions, for example, each contain a series of salinity spikes (Figure 7d) that are not associated with absolute changes in flow direction, but rather with reductions in southwestward (downriver) flow speed. As the bathymetric channel is not isolated from the surrounding water in Kotzebue Sound, a weakened outflow from the river will have more time to entrain salty ocean water along its journey from the river mouth to the measurement site, resulting in the observed salinity spikes.

Throughout the time series, rapid salinity increases are often not accompanied by a reduction in temperature, resulting in horizontal movement away from the freezing point line in temperature-salinity space (Figure 7c). This departure from the freezing point, also known as  $\Delta T$  in Section 2.3, correlates with the salinity signal processed through a simple first-order Butterworth high-pass filter to remove the longer-term trends (Figure 7f). The correlation is strongest (0.60) at a cutoff period of 3 days, but is relatively insensitive to the filter parameters, remaining above 0.50 for cutoff periods ranging between 1 and 10 days. In other words, the sensible heat content of water in the river outflow channel—reflected by  $\Delta T$ —is a function of salinity increases occurring over daily timescales (Figure 7e), which are themselves closely tied to variations in current velocity. There is residual sensible heat in some of the salty ocean water, while the rivers appear to be consistently supplying freshwater at its freezing point.

In order for heat flux to occur between the water and the ice bottom, sensible heat in the under-ice water mass must be accompanied by turbulent mixing, reflected by the friction velocity  $u_{*0}$ . Figure 8 details our application of the law of the wall to calculate  $u_{*0}$  as outlined in Section 2.3. As there are rigid boundaries at the top and bottom of the river outflow channel, we expect there to be both upper and lower boundary layers, and this is apparent from the mean velocity profiles for each flow direction (Figure 8a). The mean southwestward (downriver) flow has a shallower velocity maximum than the mean northeastward (upriver) flow, likely due to the salinity difference associated with the two flow directions. It is critical that we use only measurements from within the upper boundary layer to calculate a semi-log fit for  $u_{*0}$  and  $z_0$ , as demonstrated in panel (Figure 8b) using the mean values of all velocity measurements. Because fits to individual velocity profiles were generally quite good, we retained only those profiles with an  $R^2 > 0.9$  when constructing our friction velocity time series (Figure 8c). We then applied a 24-h centered rolling mean to better visualize events occurring on daily timescales, and to smooth out some of the variability before calculating a heat flux.

The friction velocity does not display any clear dependence on the current direction. Mean vertical gradients of horizontal velocity ( $\partial u / \partial z$ ) are nearly identical across the top meter of measurements (−0.060 m/s/m for southwestward flow, −0.063 m/s/m for northeastward flow), and correlation between  $u_{*0}$  and the depth-averaged current projected onto its primary flow axis is limited (−0.28). In general,  $u_{*0}$  is quite high throughout

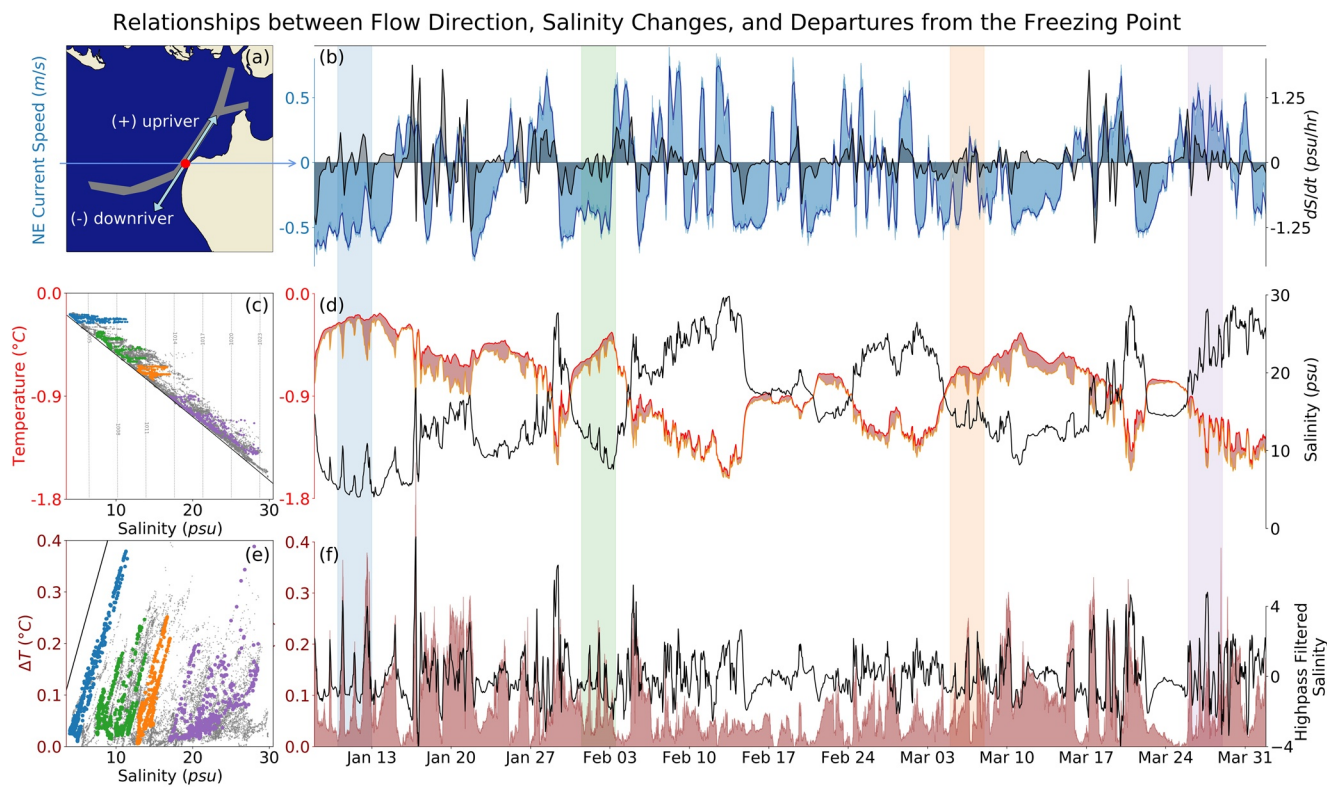


**Figure 7.** Relationships between the direction of flow in the river channel, the sign of changes in salinity, and the resulting departures of under-ice water from its freezing point. (a) Map showing the measurement site (red circle), river outflow channel (gray), and the flow directions that correspond to positive and negative values in plot (b). (b) Time series of depth-averaged current velocity, in blue, projected onto the primary flow axis (Northeast by Southwest, as shown in plot (a)). The temporal gradient of salinity is shown in black, with negative values indicating decreasing salinity over time, and positive values indicating increasing salinity over time. (c) Temperature-Salinity diagram for the water beneath the ice, with all data points plotted in gray and the four colors corresponding to the highlighted regions in the time series (plots b/d/f). Vertical dashed gray lines are density contours, and the black line shows the freezing temperature at atmospheric pressure as a function of salinity. (d) Time series of Salinity (black) and Temperature (red), with the freezing point plotted in yellow and the space between the water temperature and its freezing point shaded in dark red (this corresponds to the  $\Delta T$  parameter in plot (f)). (e) Plot of Salinity versus departure from freezing point ( $\Delta T$ ), with all data points plotted in gray and the four colors corresponding to the highlighted regions in the time series (plots b/d/f). The black line shows the relationship between Salinity and  $\Delta T$  at constant temperature. (f) Time series of departure from freezing point ( $\Delta T$ ) in dark red, equivalent to the dark red shading in plot (d). The under-ice salinity is most correlated (0.60) with  $\Delta T$  when processed through a high-pass filter with a 3-day cutoff, shown in black.

the time series regardless of flow direction, though it is worth noting that increases in  $u_{*0}$  throughout the time series are often associated with periods when the flow is reversing direction.

### 3.3. Estimating a Heat Budget for the Ice

Figure 9 shows flux balances at the top (snow-air) and bottom (water-ice) interfaces, calculated following the methods outlined in Sections 2.2 and 2.3. Calculation of the conductive flux across the snow and ice was complicated by surface flooding that began on February 14, when the weight of newly deposited snow pushed the surface of the ice below the waterline. In a companion paper to this study, Mahoney et al. (2021) present both observational and model-based evidence for the evolution of a flooded layer between the ice and dry snow. In short, the height of the ice surface above the waterline (i.e., freeboard) was determined using Archimedes' principle, our measurements of ice thickness and snow depth, and assumptions about the densities of the snow, ice, and seawater. The large storm on February 13 added enough snow to depress the ice surface below the waterline, resulting in negative freeboard and causing seawater to flood the surface of the ice. A non-waterproof temperature sensor located at the initial interface between ice and snow began giving spurious readings on February 14, which provides some observational corroboration for the timing of the expected flooding. Further accumulation of snow and thinning of the ice beneath led to continuous

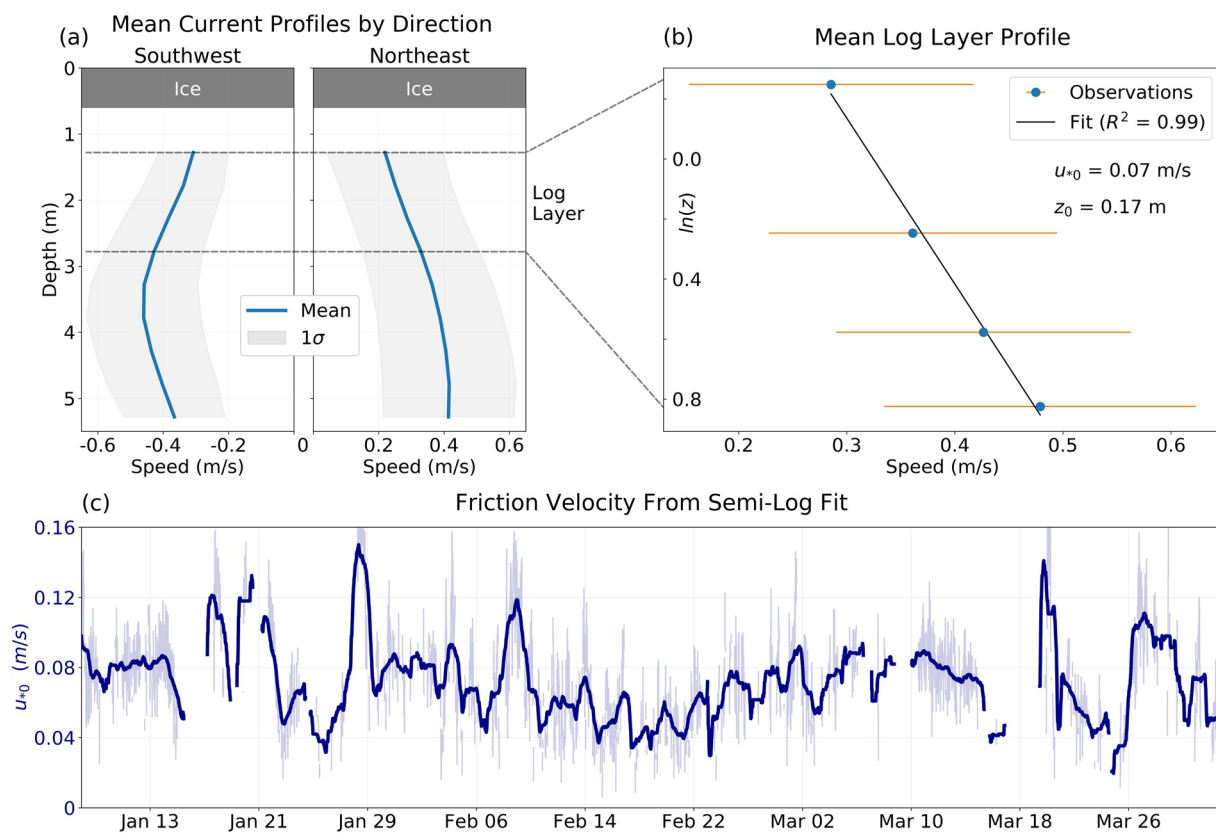


**Figure 8.** (a) Mean current profiles for the two major flow directions, showing the depth range chosen for application of the law of the wall. (b) Current speed versus the natural logarithm of the distance below the ice. Mean values are shown by blue dots, with orange bars representing 1 standard deviation of the data set. The linear fit to the mean profile in semi-log space is shown in black, along with the friction velocity and roughness length derived from the fit. (c) Time series of friction velocity derived by fitting each profile in semi-log space, as demonstrated in (b). Fitted profiles with  $R^2 < 0.9$  were excluded from the data set, resulting in a total of 3,822 data points for  $u_{*0}$ . These  $u_{*0}$  values are plotted in faded blue, while the bold blue line shows a 24-h rolling mean, which is used to calculate heat flux.

flooding that ensured the flooded layer remained partially unfrozen for the remainder of the growth season, which was confirmed during removal of the ITO. Based on these findings, Figure 9b depicts a persistent layer of liquid water at the upper surface of the ice after February 14. Under these circumstances, the sea ice below the unfrozen floodwater becomes effectively thermally decoupled from the atmosphere. With both the upper and lower surfaces of the ice in contact with seawater, they are both constrained to the freezing point, and thus the conductive flux across the ice approaches zero. Conduction of heat to the atmosphere through the snow was still calculated following Equation 3, but with  $h_i$  indicating the depth of refrozen snow-ice, and  $h_s$  the depth of dry snow above any flooding.

At the snow surface (Figure 9a), the sum total of radiative and sensible transfer remained positive—indicating that the snow surface was losing heat to the atmosphere—throughout the study period until March 21. In January and February, the total surface flux reflected a balance between sensible heat transfer and net longwave loss from the snow. The sensible heat flux was negative during periods of high outgoing LW radiation, meaning that the snow surface was radiatively cooled below the air temperature during clear-sky conditions. After March 21, the increasing input of shortwave radiation combined with the growth of the snow-ice layer led to negative surface fluxes, indicating heat transfer from the atmosphere to the snow surface and a downward conduction of heat through the dry snow and snow-ice. March 21 is also the approximate date at which the albedo began to rapidly decrease. Both of these observations imply the onset of surface melt (and non-negligible latent heat flux) in late March.

At the base of the ice (Figure 9c), the conductive flux before flooding was determined by the energy balance at the surface of the snow, based on our assumption of a linear temperature gradient through the snow and

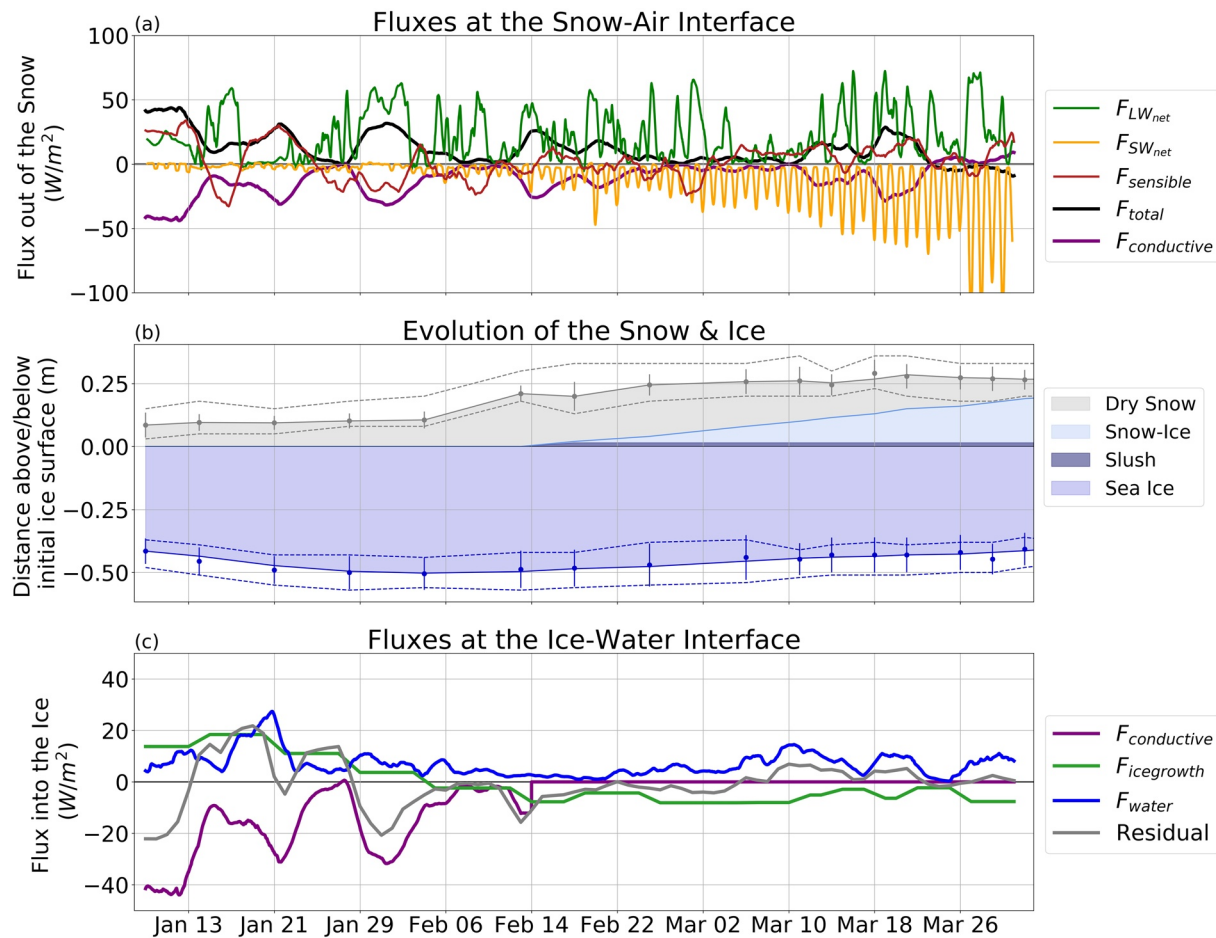


**Figure 9.** (a) Radiative and sensible fluxes at the snow surface, where a positive value indicates the transfer of heat from the snow to the atmosphere. The black line shows the sum of the radiative and sensible fluxes, which is balanced by the conductive flux as outlined in Section 2.2. A negative value for the conductive flux indicates the flow of heat from the ice bottom to the snow surface. (b) Measurements of snow and ice thickness along with the modeled evolution of the flooded layer as described in Section 3.3. Dots indicate the mean value of measurements, bars indicate the standard deviation of the measurements, and dashes indicate the maximum and minimum value of measurements. The shaded regions show the temporally smoothed values of ice and snow thickness used to calculate the conductive flux and the latent heat flux due to ice growth/melt. (c) Fluxes at the ice bottom, where a positive value indicates the transfer of heat from the water to the ice. A negative value for the conductive flux indicates the flow of heat from the ice bottom to the snow surface.

ice. Because the snow surface was always losing heat to the atmosphere throughout January and February, the conductive flux was always flowing upwards from ice bottom to snow surface, and ice growth/melt was forced by imbalances between conductive flux through the ice and water-ice heat flux at the bottom interface. After flooding, ice growth was no longer possible, and the amount of ice melt was driven by the magnitude of the water-ice heat flux. We can thus identify the turbulent transfer of heat from the water to the ice as the dominant factor inhibiting ice growth throughout our winter study period.

However, significant uncertainties in the calculation of  $F_{water}$  arose due to the magnitude of  $u_{*0}$ , which was much larger than the existing direct-covariance measurements on which our parameterization is based due to the high flow speeds in the river outflow channel. In fact, the mean “roughness Reynolds number”  $Re_* = u_{*0}z_0/v$  used in more complex parameterizations of oceanic heat flux into sea ice is approximately 73 times larger for this data set (6,600) than the median value of roughness Reynolds numbers measured across existing direct covariance data sets (90), due almost entirely to the high magnitudes of  $u_{*0}$  observed (though  $z_0$  is also approximately two times as large for our data set compared to the direct covariance data sets). As discussed in Section 2.3, the existing literature of in-situ observations (McPhee, 1987, 1992; McPhee et al., 1999, 2003; Uusikivi et al., 2006) suggest that there is no dependence of  $St_*$  on roughness Reynolds number, and the existing  $Re_*$ -dependent formulations (derived from laboratory studies) are ineffective at

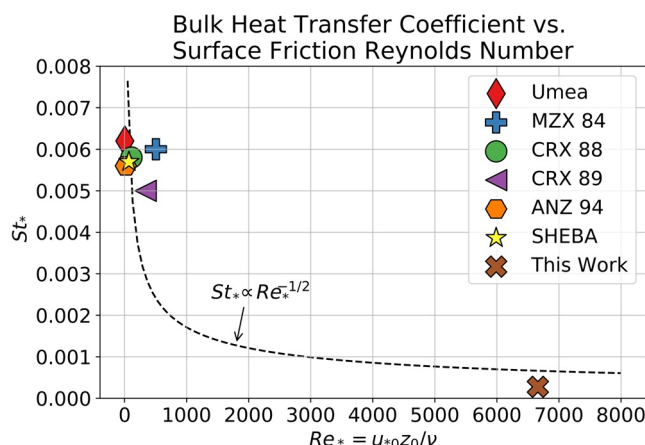


**Figure 10.**  $St_*$  versus  $Re_*$  for six experiments that made direct-covariance measurements of ocean-ice heat flux, along with the theoretical relationship of  $St_* \propto Re_*^{-1/2}$  suggested by McPhee (1992) extrapolated from the median values of these data sets ( $Re_* = 90$ ,  $St_* = 0.0057$ ). The brown X shows the location of our study in this parameter space, based on calculation of  $Re_*$  from the Law of the Wall applied to the mean current profile within the upper log layer, and calculation of  $St_*$  by minimizing the residual between the latent heat flux of ice melt (calculated from observations of ice thickness over time) and the water-ice heat flux (calculated from under-ice measurements of temperature and salinity for  $\Delta T$ , and individual profiles within the upper log layer for  $u_{*0}$ ), for the time period after the onset of flooding.

305° (southeast-northwest) axis, with significantly more flow to the northwest (leaving Kotzebue Sound) over the course of the year, corroborating our expectation that the OBT was placed in a region of net outflow from the sound. The tidal signal was much more evident in the OBT current data as compared to the ITO current data, with the dominant spectral peak occurring at the M2 harmonic period of 12.8 h. Flow direction and salinity were closely related, particularly in the fall and spring, when periods of outflow from the sound consistently led to decreases in salinity at the measurement site (Figures 11b and 11d). 14 years of moored measurements in the Bering Strait (Woodgate et al., 2005) yield climatological salinity ranges for the surface waters of the ACC of 31.4–32.6 psu in the fall, and 32.3–33.3 psu in the spring. Freshening events which correspond to periods of northwestward flow and extend well below the range of salinity climatology from the Bering Strait are likely to reflect the influence of the rivers flowing into Kotzebue Sound.

Figure 11 displays a stark contrast in the relationship between temperature and salinity in the fall as compared to the spring. In fall, freshening events corresponded to decreases in water temperature, while in spring, freshening events corresponded to increases in water temperature. Although we only have current data for the 2018/19 year with which to tie these freshening events to changes in flow direction, the seasonal contrast in the relationship between temperature and salinity was also observed in the OBT measurements from the 2017/18 deployment (Figures 11a and 11c).

## 4. Discussion

### 4.1. Seasonality of River Influence

The measurements made at these two sites allow us to piece together a picture of the interaction between river and ocean in the thermodynamics of sea ice in Kotzebue Sound. In the fall, the rivers exported freshwater that was colder than the background ocean temperature, helping to drive water temperatures in the Sound toward the (salinity-dependent) freezing point and eventually promoting sea ice growth. In the winter, river outflow was consistently at its freezing point, while salty ocean water contained some residual sensible heat, which is likely the source of heat responsible for retarding sea ice growth in the vicinity of the

predicting observational results. However, this data set is in such a different  $Re_*$  range from the literature that the  $Re_*$ -dependence anticipated from laboratory studies appears to be affecting the magnitude of our calculation for oceanic heat flux.

To produce the flux balance shown in Figure 9c, we scaled the bulk heat transfer coefficient for water-ice heat flux ( $St_*$ ) to 0.00028, 5% of its original value, to minimize the mean residual between  $F_{\text{water}}$  and  $F_{\text{icegrowth}}$  to be  $-0.1 \text{ W/m}^2$  for the period after flooding began. This scaling of  $St_*$  yields a mean residual between  $F_{\text{icegrowth}}$ ,  $F_{\text{conductive}}$ , and  $F_{\text{water}}$  before flooding of only  $-1 \text{ W/m}^2$ , suggesting that the choice of scale factor for  $F_{\text{water}}$  is reasonable and the heat budget as constructed is well-balanced over longer timescales. The assumption that there is no heat storage in the ice is likely contributing to much of the shorter timescale variability in the residual. Our scaling of  $St_*$  implies that it is approximately a factor of 20 too large for our data set, which agrees qualitatively with the inverse relationship of the form  $St_* \propto Re_*^{-1/2}$  expected from laboratory studies (McPhee, 1992). Ultimately, this study makes clear that the parameter space in Figure 10 needs to be filled out with further direct covariance measurements before a definitive statement can be made regarding the formulation of  $St_*$ .

### 3.4. Ocean Bottom Tripod Data

The ADCP on the OBT failed due to water ingress during the 2017–18 deployment, so the OBT provides us with 2 years of CTD measurements and 1 year of current profiles. The currents were bimodal along a 125–

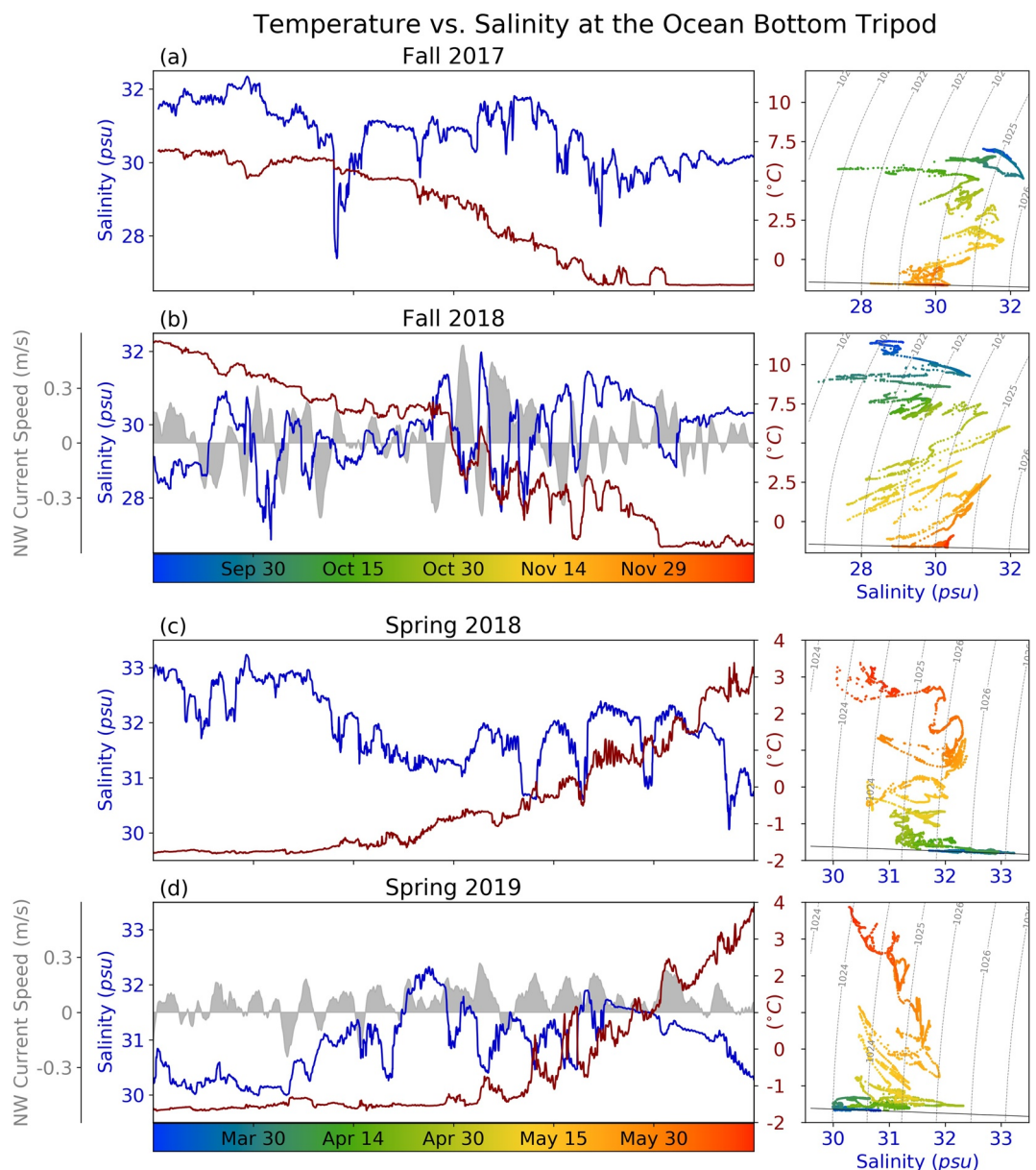


**Figure 11.** Temperature (blue) and salinity (red) measurements at the northern mouth of Kotzebue Sound for (a) Fall 2017, (b) Fall 2018, (c) Spring 2018, and (d) Spring 2019. Depth-averaged currents (gray shaded curve) are plotted along their primary flow axis (NW–SE) for the second year of measurements (b) and (d), with positive values indicating flow to the northwest out of Kotzebue Sound.

ITO (Mahoney et al., 2021). This also points to heat storage in the ocean as the primary mechanism for the unprecedented sea ice losses seen in Kotzebue Sound as well as the Bering and Chukchi Seas in the past few years, echoing other recent analyses (Huntington et al., 2020; Thoman et al., 2020). Although there have been significant positive anomalies in both air temperature and SST in this region since 2014, our observations suggest that midwinter air temperatures have not warmed to a point where they are causing a net heat input to the snow/ice from above. Rather, it is the increase in heat input to the ocean during the summer (as reflected by the SST anomalies), combined with a long-term increase in oceanic heat transport from the Pacific up through Bering Strait (Woodgate, 2018), that prevents the upper ocean from cooling all the way to its freezing point, inhibiting ice formation.

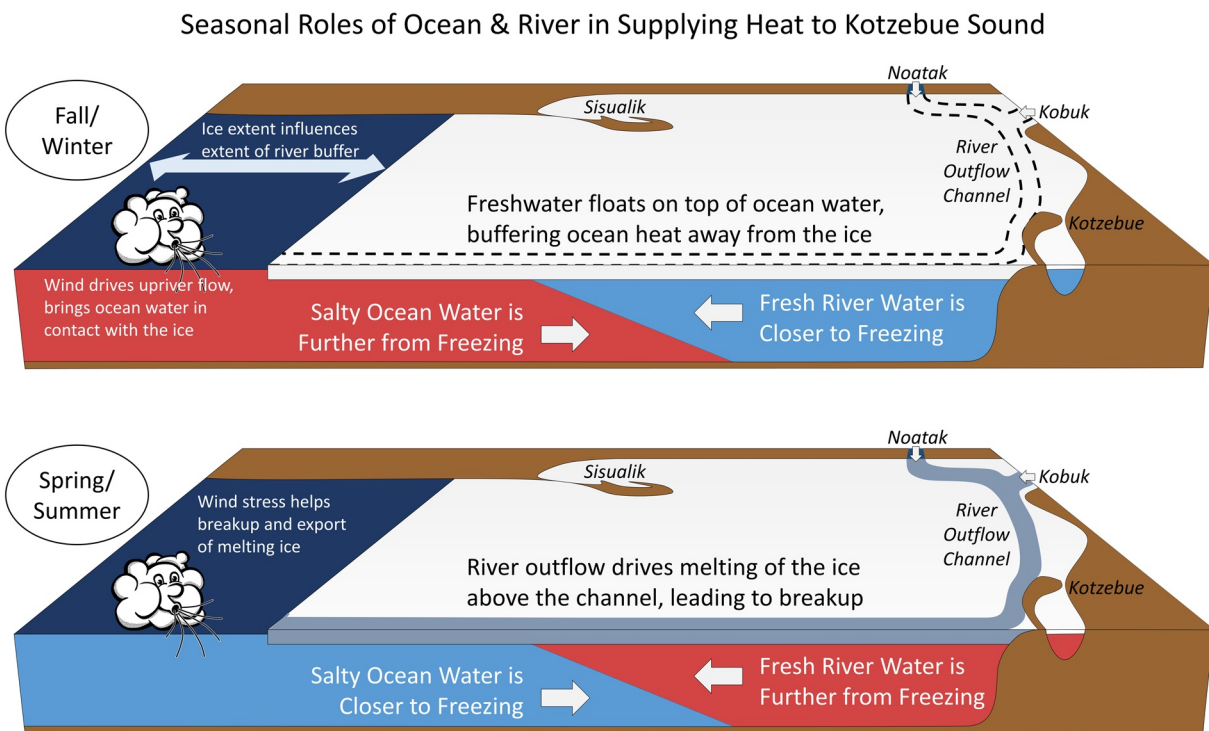


**Figure 12.** Schematic summary of the proposed understanding of seasonal differences in ocean and river heat content. In the fall and winter, the rivers export water that is closer to freezing than the ocean, positively influencing ice growth and buffering ocean water away from the ice in places where the salinity stratification is not broken down by wind. In the spring and summer, the rivers export water that is further from freezing than the ocean, helping to drive ice melt and breakup.

In the spring freshet, the rivers exported freshwater that was further from its freezing point than the ocean water, supplying additional heat energy to the water-ice interface. Although the ITO was not in place during the spring freshet, we anticipate that the freshet would be associated with increased flow speeds (and thus  $u_{*0}$ ) in the channel, further enhancing ice melt for any river water above its freezing point. As discussed in Section 1.6 and visualized in Figure 4, melting of the ice above the river outflow channel tends to precede breakup of landfast ice in Kotzebue Sound. While a definitive causal statement regarding the breakup process is beyond the scope of this study, it is clear from discussions with our Elder Advisors that loss of ice in the channel plays a role in the onset of breakup, likely via multiple factors including increased heat absorption and mechanical stress on the remaining ice. In any case, the concurrent timing between the series of warm freshwater events observed at the OBT and the opening of the river channel in mid-May (Figure 4) suggests that the river is contributing significantly to ice melt above the channel and thus helping to trigger breakup. The seasonal role reversal between ocean and rivers as heat sources to Kotzebue Sound is summarized in schematic form in Figure 12.

#### 4.2. Implications for the Local Community

Reduced ice extent in the Bering and Chukchi Seas has coincided with a number of tragic accidents involving travelers falling through landfast ice and ice on rivers (Thoman et al., 2020). The results of this study demonstrate that oceanic heat can affect inland ice where a channel provides a pathway for tidal fluxes. Our results also suggest that riverine heat contributes to thinning of coastal sea ice once river water temperatures rise above freezing. Because of the extremely shallow bathymetry in the northeast corner of Kotzebue Sound, grounded landfast ice seems likely to persist in this region even in years where residual ocean heat inhibits the formation of any other sea ice. This bottom fast ice in the northeast corner of the Sound (and in the lakes behind the Kotzebue peninsula) provides a winter bridge between Kotzebue and neighboring communities such as Selawik and Sisualik, enabling people to make on-ice journeys that require an expensive boat or plane ride in other seasons. However, a future scenario in which the rivers do not remain at

the freezing point throughout the winter would put the persistence of this ice in jeopardy. Real-time monitoring of rivers to detect the onset of thawing temperatures upstream may therefore provide a robust and relatively low-cost mechanism for predicting unsafe ice conditions in the immediate vicinity of Kotzebue. These upstream measurements could be paired with the ongoing community-based measurements of snow and ice thickness and under-ice water temperature and salinity in the Sound (initiated by Ikaágvik Sikukun and now maintained by a community-based monitoring program called the Alaska Arctic Observatory and Knowledge Hub, or AAOKH) to give a relatively complete picture of the state of Kotzebue Sound sea ice throughout each winter.

“Sea ice is the freedom-bringer” (Gearheard et al., 2013) not only for humans but for migrating *tuttu* (Iñupiaq for caribou, *Rangifer tarandus*) as well, some of whom use the sea ice in the eastern margins of Kotzebue Sound as a bridge to shorten their journey from the Seward Peninsula to their calving grounds on the North Slope (Joly, 2013). Tracking upstream river conditions—as a measure of how early these ice bridges become completely impassable—could thus be a predictor for the number of *tuttu* forced to summer on the Seward peninsula.

The landfast ice also provides habitat for both *natchiq* and *ugruk* (Iñupiaq for ringed seals, *Phoca hispida*, and bearded seals, *Erignathus barbatus*, respectively), important sources of food, oil, and warm clothing for the Indigenous inhabitants of Kotzebue (Huntington, Nelson, et al., 2016). The life histories of both species are uniquely adapted to use sea ice for reproduction, resting, molting, and as a platform from which to forage, which contribute to concerns about population viability and resilience to sea ice reduction (Laidre et al., 2015; Moore & Reeves, 2018). Limited data preclude analyses of population numbers or trends of these species in the Pacific Arctic region (Conn et al., 2014), although subsistence harvests remain sustainable (Nelson et al., 2019). Body condition and other metrics also suggest there have so far been limited biological responses to environmental change (Crawford et al., 2015). Ultimately, while hunters report that these seals have remained available in recent years, hunting conditions have changed dramatically (Huntington et al., 2017). *Ugruk* are of particular importance due to their enormous size, and are primarily hunted from boats after the ice has started to break up, a time of year when the seals spend hours hauled out on ice edges (Huntington, Quakenbush, et al., 2016). For the community of Kotzebue, the onset of *ugruk* hunting season is determined by the breakup of the river channel, which has trended slightly earlier over the past 17 years (Hauser et al., 2021). However, the loss of ice in the Sound has led to a dramatic reduction in the overall length of the hunting season, as the window of time when it is possible to launch a boat from Kotzebue while there is still ice in the Sound shrinks (Hauser et al., 2021; Huntington, Quakenbush, & Nelson, 2016). Real-time monitoring of upstream river temperatures would help give hunters in Kotzebue advance warning of the onset of *ugruk* hunting season, facilitating the community’s continued access to this important subsistence resource as the window for a successful harvest narrows. Thus far, hunters have been able to modify their efforts, maintaining successful harvests despite rapidly changing ice conditions and shortened harvest periods, but it remains unclear if future conditions will continue to provide access for hunters (Hauser et al., 2021).

#### 4.3. Implications for the Arctic

The results of this study also highlight the importance of terrestrial forcing via rivers in coastal sea ice dynamics throughout the Arctic, where several of the world’s largest rivers empty into regions populated by communities and cultures that are tied to the sea ice. It is difficult to generalize the relationship between river discharge and ice extent based on the existing literature, as some studies have reported a negative correlation (Bareiss et al., 1999; Ogi et al., 2001) and others a positive correlation (Holt et al., 1984; Manak & Mysak, 1989) depending on the region and scale of the study. While most studies have hypothesized that river discharge should have different effects on sea ice in the fall and spring, few have undertaken detailed examination of this relationship at sub-yearly timescales. Our measurements have demonstrated that river discharge can promote both ice formation and ice melt depending on the time of year, thus correlations between yearly anomalies reported in previous studies will simply reflect whichever effect is dominant over a yearly cycle in that region.

Studies of the outflow region of the Lena River into the Laptev Sea have found that landfast ice in the immediate vicinity of the outflow was primarily influenced by processes upstream, and unlikely to be sensitive

to the timing of melt onset driven by ocean or atmosphere near the river mouth (Bareiss et al., 1999; Bauch et al., 2013). This has likely also been the case historically in Kotzebue Sound—as river discharge spreads out beneath the landfast ice, it will create a freshwater “blanket” between the salinity-stratified ocean below and the ice above, thus exerting control over sensible heat input to the ice bottom. The spatial extent of the rivers’ influence will be dependent on how far the freshwater can spread below the ice before encountering open water, where wind-driven mixing will weaken the stratification between water masses. Our observations suggest that this freshwater blanket exerts a stabilizing effect on the landfast ice during winter by buffering residual ocean heat away from the surface, promoting ice growth in winter and retarding bottom melt in early summer. However, we also observed ocean heat coming into contact with the ice bottom throughout our study period, perhaps as a result of increased wind-driven mixing within Kotzebue Sound enabled by the anomalously low landfast ice extent. These observations provide evidence that a positive feedback loop exists here, in which shrinking landfast ice cover decreases the geographic extent of the rivers’ stabilizing influence, allowing ocean heat to come into contact with the ice during winter and further inhibiting landfast ice growth (Figure 12). This feedback between landfast ice extent and stabilizing river influence is likely a generalizable phenomenon for any Arctic river that consistently exports water at its freezing point throughout the winter.

As Arctic sea ice cover continues to shrink, landfast ice persisting in coastal margins is expected to become centrally important to the persistence and resilience of ice-dependent marine mammals and the subsistence hunters who rely on them (Moore & Reeves, 2018). However, the landfast ice season in the Chukchi Sea has itself been shrinking by approximately 1 week per decade (Mahoney et al., 2014). Further year-round observation and satellite-based modeling (such as in Searcy et al., 1996) of the influence of river outflow on the landfast ice season is needed to accurately predict the persistence or loss of this ice throughout the major Arctic river basins.

## 5. Conclusion

Measurements of radiative and sensible fluxes, ice and snow mass balance, and underwater temperature, salinity, and current profiles were combined to quantify the heat budget of landfast ice in Kotzebue Sound. These measurements identified the ocean as the main source of heat to the ice during the winter. This suggests oceanic heat as the primary driver for the unprecedented sea ice minima seen in 2018 and 2019 in the Bering and Chukchi Seas, and further suggests that SST anomalies and heat transport through the Bering Strait during summer are likely preconditioning factors for ice cover in Kotzebue Sound the following year. The measurements also revealed a striking seasonal pattern in the effect of the river outflows: promoting ice formation and stability during fall and winter, but helping to drive ice melt in spring. The fall/winter effect aided the persistence of landfast ice grounded on shallow bathymetry in the vicinity of the river outflow during years in which no other sea ice was present in Kotzebue Sound. This result implies that landfast ice is likely to persist in the shallow margins of the Sound as long as the rivers are cooled to their freezing point during the fall season, providing habitat and hunting grounds to marine mammals and subsistence hunters. Furthermore, we propose real-time monitoring of upstream temperatures as a robust and relatively low-cost predictor for unsafe spring ice conditions and the opening of the river channel, with the potential to both save lives and assist hunters in their preparation for the shrinking *ugruk* hunt season. Finally, the results of this study make clear that it is critical to consider the seasonality of river-ice interactions throughout the Arctic, and that predictions made regarding coastal ice thermodynamics are unlikely to be skillful if the influence of rivers is not taken into account. These predictions are needed by communities throughout the Arctic that rely on coastal sea ice to provide transportation, food, and clothing. Future terrestrial warming may significantly diminish what positive influence rivers do exert on ice growth. For now, it appears that rivers provide a bastion during the fall against the rapid sea ice loss occurring in the basin, helping a small piece of the Arctic garden to endure even if the rest has disappeared.

## Conflict of Interest

The authors declare no conflicts of interest relevant to this study.

## Data Availability Statement

Data supporting the conclusions made in this study are archived on Columbia Academic Commons (ITO: <https://doi.org/10.7916/d8-c78w-cd84>; FWS Radiometers: <https://doi.org/10.7916/d8-9sgf-nh46>; OBT: <https://doi.org/10.7916/d8-emgj-j795>).

## Acknowledgments

This work was supported by a research grant from the Gordon and Betty Moore Foundation. The authors are grateful to the Qikiqtaalukmiut people and community of Kotzebue for sharing their Indigenous Knowledge and welcoming our research team. In particular, the authors wish to thank Pearl Goodwin, Siikauraq Whiting, and Vernetta Nay Moberly for their support and generosity. The authors also extend our gratitude to the Native Village of Kotzebue, the University of Alaska Fairbanks Chukchi campus, and the US Fish and Wildlife Selawik Refuge. Finally, the authors would like to thank our reviewers for their detailed feedback and recommendations, which greatly improved this manuscript.

## References

- Aagaard, K., & Carmack, E. C. (1989). The role of sea ice and other fresh water in the Arctic circulation. *Journal of Geophysical Research*, 94(C10), 14485–14498. <https://doi.org/10.1029/JC094iC10p14485>
- Ahlnas, K., & Garrison, G. R. (1984). Satellite and oceanographic observations of the warm coastal current in the Chukchi Sea. *Arctic*, 37(3), 244–254. <https://doi.org/10.14430/arctic2197>
- Andreas, E. L. (2002). Parameterizing scalar transfer over snow and ice: A review. *Journal of Hydrometeorology*, 3(4), 417–432. [https://doi.org/10.1175/1525-7541\(2002\)003<0417:PSTOSA>2.0.CO;2](https://doi.org/10.1175/1525-7541(2002)003<0417:PSTOSA>2.0.CO;2)
- Andreas, E. L., Jordan, R. E., & Makshtas, A. P. (2005). Parameterizing turbulent exchange over sea ice: The ice station Weddell results. *Boundary-Layer Meteorology*, 114(2), 439–460. <https://doi.org/10.1007/s10546-004-1414-7>
- Bareiss, J., Eicken, H., Helbig, A., & Martin, T. (1999). Impact of river discharge and regional climatology on the decay of sea ice in the Laptev Sea during spring and early summer. *Arctic Antarctic, and Alpine Research*, 31(3), 214–229. <https://doi.org/10.1080/15230430.1999.12003302>
- Bauch, D., Hölemann, J. A., Nikulina, A., Wegner, C., Janout, M. A., Timokhov, L. A., & Kassens, H. (2013). Correlation of river water and local sea-ice melting on the Laptev Sea shelf (Siberian Arctic). *Journal of Geophysical Research: Oceans*, 118(1), 550–561. <https://doi.org/10.1002/jgrc.20076>
- Behe, C., & Daniel, R. (2018). Indigenous knowledge and the co-production of knowledge process: Creating a holistic understanding of arctic change.[in 'State of the Climate in 2017']. *Bulletin of the American Meteorological Society*, 99(8), S160–S161.
- Boé, J., Hall, A., & Qu, X. (2009). September sea-ice cover in the Arctic Ocean projected to vanish by 2100. *Nature Geoscience*, 2(5), 341–343. <https://doi.org/10.1038/ngeo467>
- Bronen, R. (2010). Forced migration of Alaskan indigenous communities due to climate change. In T. Afifi, & J. Jäger (Eds.), *Environment, forced migration and social vulnerability* (pp. 87–98). Berlin, Heidelberg: Springer. [https://doi.org/10.1007/978-3-642-12416-7\\_7](https://doi.org/10.1007/978-3-642-12416-7_7)
- Coachman, L. K., Coachman, L. K., Aagaard, K., & Tripp, R. B. (1975). *Bering Strait: The regional physical oceanography*. University of Washington Press.
- Conn, P. B., Hoef, J. M. V., McClintock, B. T., Moreland, E. E., London, J. M., Cameron, M. F., et al. (2014). Estimating multispecies abundance using automated detection systems: Ice-associated seals in the Bering Sea. *Methods in Ecology and Evolution*, 5(12), 1280–1293. <https://doi.org/10.1111/2041-210X.12127>
- Crawford, J. A., Quakenbush, L. T., & Citta, J. J. (2015). A comparison of ringed and bearded seal diet, condition and productivity between historical (1975–1984) and recent (2003–2012) periods in the Alaskan Bering and Chukchi seas. *Progress in Oceanography*, 136, 133–150. <https://doi.org/10.1016/j.pocean.2015.05.011>
- Dai, A., Luo, D., Song, M., & Liu, J. (2019). Arctic amplification is caused by sea-ice loss under increasing CO<sub>2</sub>. *Nature Communications*, 10(1), 1–13. <https://doi.org/10.1038/s41467-018-07954-9>
- Eicken, H. (2010). Indigenous knowledge and sea ice science: What can we learn from indigenous ice users? In I. Krupnik, C. Aporta, S. Gearheard, G. J. Laidler, & L. Kielsen Holm (Eds.), *SIKU: Knowing our ice: Documenting inuit sea ice knowledge and use* (pp. 357–376). Dordrecht: Springer Netherlands. [https://doi.org/10.1007/978-90-481-8587-0\\_15](https://doi.org/10.1007/978-90-481-8587-0_15)
- Fang, Z., Freeman, P. T., Field, C. B., & Mach, K. J. (2018). Reduced sea ice protection period increases storm exposure in Kivalina, Alaska. *Arctic Science (World)*, 4, 525–537. <https://doi.org/10.1139/as-2017-0024>
- Francis, J. A., & Vavrus, S. J. (2015). Evidence for a wavier jet stream in response to rapid Arctic warming. *Environmental Research Letters*, 10(1), 014005. <https://doi.org/10.1088/1748-9326/10/1/014005>
- Gearheard, S., Holm, L. K., & Huntington, H. P. (2013). *The meaning of ice: People and sea ice in three Arctic communities*. International Polar Institute Press.
- Hauser, D. D. W., Whiting, A. V., Mahoney, A. R., Goodwin, J., Harris, C., Schaeffer, R. J., et al. (2021). Co-production of knowledge reveals loss of Indigenous hunting opportunities in the face of accelerating Arctic climate change. *Environmental Research Letters*, 16(9), 095003. <https://doi.org/10.1088/1748-9326/ac1a36>
- Holland, M. M., & Bitz, C. M. (2003). Polar amplification of climate change in coupled models. *Climate Dynamics*, 21(3), 221–232. <https://doi.org/10.1007/s00382-003-0332-6>
- Holt, T., Kelly, P. M., & Cherry, B. S. G. (1984). Cryospheric impacts of Soviet River diversion schemes. *Annals of Glaciology*, 5, 61–68. <https://doi.org/10.3189/1984AoG5-1-61-68>
- Huntington, H. P., Danielson, S. L., Wiese, F. K., Baker, M., Boveng, P., Citta, J. J., et al. (2020). Evidence suggests potential transformation of the Pacific Arctic ecosystem is underway. *Nature Climate Change*, 10(4), 342–348. <https://doi.org/10.1038/s41558-020-0695-2>
- Huntington, H. P., Nelson, M., & Quakenbush, L. T. (2016a). Traditional knowledge regarding ringed seals, bearded seals, and walrus near Kotzebue, Alaska. Final report to the Eskimo Walrus Commission, the Ice Seal Committee, and the Bureau of Ocean Energy Management for contract.
- Huntington, H. P., Quakenbush, L. T., & Nelson, M. (2016b). Effects of changing sea ice on marine mammals and subsistence hunters in northern Alaska from traditional knowledge interviews. *Biology Letters*, 12(8), 20160198. <https://doi.org/10.1098/rsbl.2016.0198>
- Huntington, H. P., Quakenbush, L. T., & Nelson, M. (2017). Evaluating the effects of climate change on indigenous marine mammal hunting in Northern and Western Alaska using traditional knowledge. *Frontiers in Marine Science*, 4, 319. <https://doi.org/10.3389/fmars.2017.00319>
- Joly, K. (2013). Sea ice crossing by migrating Caribou, *Rangifer tarandus*, in Northwestern Alaska. *Canadian Field-Naturalist*, 126(3), 217–220. <https://doi.org/10.22621/cfn.v126i3.1363>
- Klenk, N., Fiame, A., Meehan, K., & Gibbes, C. (2017). Local knowledge in climate adaptation research: Moving knowledge frameworks from extraction to co-production. *WIREs Climate Change*, 8(5), e475. <https://doi.org/10.1002/wcc.475>
- Kondo, J., & Yamazawa, H. (1986). Bulk transfer coefficient over a snow surface. *Boundary-Layer Meteorology*, 34(1), 123–135. <https://doi.org/10.1007/BF00120912>

- LaFond, E. C. (1954). Physical oceanography and submarine geology of the seas to the West and North of Alaska. *Arctic*, 7(2), 93–101. <https://doi.org/10.14430/arctic3832>
- Laidre, K. L., Stern, H., Kovacs, K. M., Lowry, L., Moore, S. E., Regehr, E. V., et al. (2015). Arctic marine mammal population status, sea ice habitat loss, and conservation recommendations for the 21st century. *Conservation Biology*, 29(3), 724–737. <https://doi.org/10.1111/cobi.12474>
- Laxon, S. W., Giles, K. A., Ridout, A. L., Wingham, D. J., Willatt, R., et al. (2013). CryoSat-2 estimates of Arctic sea ice thickness and volume. *Geophysical Research Letters*, 40(4), 732–737. <https://doi.org/10.1029/grl.50193>
- Mahoney, A. R., Eicken, H., Gaylord, A. G., & Gens, R. (2014). Landfast sea ice extent in the Chukchi and Beaufort Seas: The annual cycle and decadal variability. *Cold Regions Science and Technology*, 103, 41–56. <https://doi.org/10.1016/j.coldregions.2014.03.003>
- Mahoney, A. R., Gearheard, S., Oshima, T., & Qillaq, T. (2009). Sea ice thickness measurements from a community-based observing network. *Bulletin of the American Meteorological Society*, 90(3), 370–378. <https://doi.org/10.1175/2008BAMS2696.1>
- Mahoney, A. R., Turner, K., Hauser, D. D. W., Laxague, N. J. M., Lindsay, J. M., Whiting, A. V., et al. (2021). Thin ice, deep snow, and surface flooding: The mass balance of landfast ice in Kotzebue Sound during two anomalously warm winters. *Journal of Glaciology*, 1–15. <https://doi.org/10.1017/jog.2021.49>
- Manak, D. K., & Mysak, L. A. (1989). On the relationship between arctic sea-ice anomalies and fluctuations in Northern Canadian air temperature and river discharge. *Atmosphere-Ocean*, 27(4), 682–691. <https://doi.org/10.1080/07055900.1989.9649361>
- Maykut, G. A. (1986). The surface heat and mass balance. In N. Untersteiner (Ed.), *The geophysics of sea ice* (pp. 395–463). Boston, MA: Springer US. [https://doi.org/10.1007/978-1-4899-5352-0\\_6](https://doi.org/10.1007/978-1-4899-5352-0_6)
- McGillis, W. R., Edson, J. B., Zappa, C. J., Ware, J. D., McKenna, S. P., et al. (2004). Air-sea CO<sub>2</sub> exchange in the equatorial Pacific. *Journal of Geophysical Research*, 109(C8), C08S02. <https://doi.org/10.1029/2003JC002256>
- McPhee, M. G. (1987). A time-dependent model for turbulent transfer in a stratified oceanic boundary layer. *Journal of Geophysical Research*, 92(C7), 6977. <https://doi.org/10.1029/JC092iC07p06977>
- McPhee, M. G. (1992). Turbulent heat flux in the upper ocean under sea ice. *Journal of Geophysical Research*, 97(C4), 5365–5379. <https://doi.org/10.1029/92JC00239>
- McPhee, M. G. (2008). *Air-ice-ocean interaction: Turbulent ocean boundary layer exchange processes*. Springer Science & Business Media.
- McPhee, M. G., Kikuchi, T., Morison, J. H., & Stanton, T. P. (2003). Ocean-to-ice heat flux at the North Pole environmental observatory. *Geophysical Research Letters*, 30(24), 2274. <https://doi.org/10.1029/2003GL018580>
- McPhee, M. G., Kottmeier, C., & Morison, J. H. (1999). Ocean heat flux in the Central Weddell Sea during winter. *Journal of Physical Oceanography*, 29(6), 1166–1179. [https://doi.org/10.1175/1520-0485\(1999\)029<1166:OHFTC>2.0.CO;2](https://doi.org/10.1175/1520-0485(1999)029<1166:OHFTC>2.0.CO;2)
- Moore, S. E., & Reeves, R. R. (2018). Tracking arctic marine mammal resilience in an era of rapid ecosystem alteration. *PLOS Biology*, 16(10), e2006708. <https://doi.org/10.1371/journal.pbio.2006708>
- Nelson, M. A., Quakenbush, L. T., Taras, B. D., & Committee, I. S. (2019). Subsistence harvest of ringed, bearded, spotted, and ribbon seals in Alaska is sustainable. *Endangered Species Research*, 40, 1–16. <https://doi.org/10.3354/esr00973>
- Ogi, M., Tachibana, Y., Nishio, F., & Danchenkov, M. A. (2001). Does the fresh water supply from the Amur River flowing into the Sea of Okhotsk affect sea ice formation? *Journal of the Meteorological Society of Japan Ser II*, 79(1), 123–129. <https://doi.org/10.2151/jmsj.79.123>
- Overland, J. E., & Wang, M. (2013). When will the summer Arctic be nearly sea ice free? *Geophysical Research Letters*, 40(10), 2097–2101. <https://doi.org/10.1029/grl.50316>
- Overpeck, J. T., Sturm, M., Francis, J. A., Perovich, D. K., Serreze, M. C., Benner, R., et al. (2005). Arctic system on trajectory to new, seasonally ice-free state. *Eos, Transactions American Geophysical Union*, 86(34), 309–313. <https://doi.org/10.1029/2005EO340001>
- Owen, P. R., & Thomson, W. R. (1963). Heat transfer across rough surfaces. *Journal of Fluid Mechanics*, 15(3), 321–334. <https://doi.org/10.1017/S0022112063000288>
- Park, H., Watanabe, E., Kim, Y., Polyakov, I., Oshima, K., Zhang, X., et al. (2020). Increasing riverine heat influx triggers Arctic sea ice decline and oceanic and atmospheric warming. *Science Advances*, 6(45), eabc4699. <https://doi.org/10.1126/sciadv.abc4699>
- Perovich, D., Meier, W., Tschudi, M., Farrell, S., Hendricks, S., Gerland, S., & Webster, M. (2018). Sea ice. In E. Osborne, J. Richter-Menge, & M. Jeffries (Eds.), *Arctic report card 2018*. Retrieved from <https://www.arctic.noaa.gov/Report-Card>
- Pistone, K., Eisenman, I., & Ramanathan, V. (2019). Radiative heating of an ice-free Arctic Ocean. *Geophysical Research Letters*, 46(13), 7474–7480. <https://doi.org/10.1029/2019GL082914>
- Schweiger, A., Lindsay, R., Zhang, J., Steele, M., Stern, H., & Kwok, R. (2011). Uncertainty in modeled Arctic sea ice volume. *Journal of Geophysical Research*, 116, C00D06. <https://doi.org/10.1029/2011JC007084>
- Screen, J. A., & Simmonds, I. (2010). The central role of diminishing sea ice in recent Arctic temperature amplification. *Nature*, 464(7293), 1334–1337. <https://doi.org/10.1038/nature09051>
- Searcy, C., Dean, K., & Stringer, W. (1996). A river-coastal sea ice interaction model: Mackenzie River Delta. *Journal of Geophysical Research*, 101(C4), 8885–8894. <https://doi.org/10.1029/96JC00120>
- Stroeve, J., Holland, M. M., Meier, W., Scambos, T., & Serreze, M. (2007). Arctic sea ice decline: Faster than forecast. *Geophysical Research Letters*, 34(9), L09501. <https://doi.org/10.1029/2007GL029703>
- Thoman, R. L., Bhatt, U. S., Bieniek, P. A., Brettschneider, B. R., Brubaker, M., Danielson, S. L., et al. (2020). The record low Bering Sea ice extent in 2018: Context, impacts, and an assessment of the role of anthropogenic climate change. *Bulletin of the American Meteorological Society*, 101(1), S53–S58. <https://doi.org/10.1175/BAMS-D-19-0175.1>
- Timmermans, M. L., & Ladd, C. (2019). Sea surface temperature. In J. Richter-Menge, M. L. Druckenmiller, & M. Jeffries (Eds.), *Arctic report card 2019*. Retrieved from <http://www.arctic.noaa.gov/Report-Card>
- Uusikivi, J., Ehn, J., & Granskog, M. A. (2006). Direct measurements of turbulent momentum, heat and salt fluxes under landfast ice in the Baltic Sea. *Annals of Glaciology*, 44, 42–46. <https://doi.org/10.3189/172756406781811150>
- Whitefield, J., Winsor, P., McClelland, J., & Menemenlis, D. (2015). A new river discharge and river temperature climatology data set for the pan-Arctic region. *Ocean Modelling*, 88, 1–15. <https://doi.org/10.1016/j.ocemod.2014.12.012>
- Woodgate, R. A. (2018). Increases in the Pacific inflow to the Arctic from 1990 to 2015, and insights into seasonal trends and driving mechanisms from year-round Bering Strait mooring data. *Progress in Oceanography*, 160, 124–154. <https://doi.org/10.1016/j.pocean.2017.12.007>
- Woodgate, R. A., Aagaard, K., & Weingartner, T. J. (2005). Monthly temperature, salinity, and transport variability of the Bering Strait through flow. *Geophysical Research Letters*, 32(4), L04601. <https://doi.org/10.1029/2004GL021880>
- Yaglom, A. M., & Kader, B. A. (1974). Heat and mass transfer between a rough wall and turbulent fluid flow at high Reynolds and Péclet numbers. *Journal of Fluid Mechanics*, 62(3), 601–623. <https://doi.org/10.1017/S0022112074000838>